REPORT DOCUMENTATION PAGE

AFRL-SR-AR-TR-05-

0369

PLEASE DO NOT RETURN YOUR FORM TO THE ABOVE ADDRESS.

1. REPORT DATE *(DD-MM-YYYY)*	2. REPORT TYPE	3. DATES COVERED *(From - To)*
	Final Report	01 Apr 2002 - 31 Dec 2004

4. TITLE AND SUBTITLE

Experimental and Computational Study of the Effect of MHD Forces on Stability and Separation of Nonequilibrium Ionized Supersonic Flow

5a. CONTRACT NUMBER

5b. GRANT NUMBER

F49620-02-1-0164

5c. PROGRAM ELEMENT NUMBER

6. AUTHOR(S)

Dr. Igor V. Adamovich

5d. PROJECT NUMBER

5e. TASK NUMBER

5f. WORK UNIT NUMBER

7. PERFORMING ORGANIZATION NAME(S) AND ADDRESS(ES)

Department of Mechanical Engineering
The Ohio State University
Columbus OH 43210

8. PERFORMING ORGANIZATION REPORT NUMBER

9. SPONSORING/MONITORING AGENCY NAME(S) AND ADDRESS(ES)

USAF/AFRL
AFOSR
875 North Randolph Street
Arlington VA 22203

NA

10. SPONSOR/MONITOR'S ACRONYM(S)

AFOSR

11. SPONSOR/MONITOR'S REPORT NUMBER(S)

12. DISTRIBUTION/AVAILABILITY STATEMENT

Distribution Statement A. Approved for public release; distribution is unlimited.

13. SUPPLEMENTARY NOTES

14. ABSTRACT

The results of the present work demonstrate the Lorentz force effect on the supersonic boundary layer in M=3 flows of nitrogen ionized by a transverse RF discharge in the presence of the magnetic field. Boundary layer density fluctuation spectra are measured using the Laser Differential Interferometry (LDI) diagnostics. In particular, decelerating Lorentz force applied to the flow produces a well reproduced increase of the density fluctuation intensity by up to 10-20% (1-2 dB), compared to the accelerating force of the same magnitude applied to the same flow. The effect is produced for two possible combinations of the magnetic field and MHD current directions producing the same Lorentz force direction (both for accelerating and decelerating force). The effect is observed to increase with the flow conductivity.

15. SUBJECT TERMS

16. SECURITY CLASSIFICATION OF:			17. LIMITATION OF ABSTRACT	18. NUMBER OF PAGES	19a. NAME OF RESPONSIBLE PERSON
a. REPORT	b. ABSTRACT	c. THIS PAGE			19b. TELEPHONE NUMBER *(Include area code)*
U	U	U	UU	49	

EXPERIMENTAL AND COMPUTATIONAL STUDY OF THE EFFECT OF MHD FORCES ON STABILITY AND SEPARATION OF NONEQUILIBRIUM IONIZED SUPERSONIC FLOW

(F49620-02-1-0164)

Igor V. Adamovich, J. William Rich, and Vish Subramaniam

Department of Mechanical Engineering

The Ohio State University, Columbus, OH 43210

EXECUTIVE SUMMARY

A new blowdown nonequilibrium plasma MHD supersonic wind tunnel operated at complete steady state has been developed and tested at Ohio State. The wind tunnel can be operated at Mach numbers up to M=3-4, and mass flow rates of up to 45 g/sec at a stagnation pressure of 1 atm. Pitot tube and schlieren measurements in a M=3 test section showed reasonably good flow quality, up to 80% inviscid core across the larger dimension and up to 50% inviscid core across the smaller dimension of the flow. Stable and diffuse transverse RF discharges (RF power up to 1 kW) have been sustained in M=3 nitrogen flows, at magnetic fields of up to B=1.5 T. Operation at higher magnetic fields produced a more uniform RF plasma in the MHD test section. The results of the present work demonstrate the Lorentz force effect on the supersonic boundary layer in M=3 flows of nitrogen ionized by a transverse RF discharge in the presence of the magnetic field. Boundary layer density fluctuation spectra are measured using the Laser Differential Interferometry (LDI) diagnostics. In particular, decelerating Lorentz force applied to the flow produces a well reproduced increase of the density fluctuation intensity by up to 10-20% (1-2 dB), compared to the accelerating force of the same magnitude applied to the same flow. The effect is produced for two possible combinations of the magnetic field and MHD current directions producing the same Lorentz force direction (both for accelerating and decelerating force). The effect is observed to increase with the flow conductivity.

The report summarizes results of magnetohydrodynamic (MHD) supersonic boundary layer control experiments using repetitively pulsed, short pulse duration, high voltage discharges in M=3 flows of nitrogen and air in the presence of a magnetic field of B=1.5 T. Boundary layer flow visualization experiments using laser sheet scattering are also presented. Flow visualization shows that side wall boundary layers in the supersonic test section are considerably thicker near the center plane of the flow. The results also show that as the Reynolds number increases from $Re_x=2.7\cdot10^5$ to $8.1\cdot10^5$, the boundary layer flow becomes much more chaotic, with the spatial scale of temperature fluctuations decreasing. Combined with density fluctuation spectra measurements using LDI diagnostics, this behavior suggests that boundary layer transition occurs at stagnation pressures of P_0~200-250 torr. Operation of a crossed discharge (pulser + DC sustainer) in M=3 flows of air and nitrogen demonstrated that such a discharge produces a stable, diffuse, and uniform plasma. The time-average DC current achieved in such discharges is up to 1.0 A in nitrogen (conductivity of σ=0.073 mho/m) and up to 0.8 A in air (σ=0.072 mho/m). The electrical conductivity and the Hall parameter in nitrogen and air flows are inferred from the

current voltage characteristics of the sustainer discharge. LDI measurements detected MHD effect on the ionized boundary layer density fluctuations at these conditions. Retarding Lorentz force applied to M=3 nitrogen, air, and N_2-He flows produces an increase of the density fluctuation intensity by up to 2 dB (about 25%), compared to the accelerating force of the same magnitude. The effect is demonstrated for two possible combinations of the magnetic field and current directions producing the same Lorentz force direction (both for accelerating and retarding force). Comparison with the LDI spectra measured with no MHD force applied showed that the effect on the density fluctuations is produced only by the retarding Lorentz force, while the Joule heat effect appears insignificant.

The results of this research reflect close collaboration with Air Vehicles Directorate of AFRL (Dr. Roger Kimmel), AFIT (Dr. R. McMullan), and UCLA (Prof. X. Zhong) and are published in 2 journal papers and presented in 7 contributed papers at AIAA Plasmadynamics and Lasers Conferences.

CHAPTER I. MEASUREMENTS OF FLOW CONDUCTIVITY AND DENSITY FLUCTUATIONS IN SUPERSONIC NONEQUILIBRIUM MHD FLOWS IONIZED BY TRANSVERSE RF DISCHARGE

1. Introduction

The use of magnetohydrodynamics for supersonic flow control, supersonic air-breathing propulsion, and for development of novel hypersonic ground testing facilities continues to attract considerable interest [1-5]. The most serious challenge in developing these applications is creating and sustaining electrical conductivity in the airflow sufficient to produce substantial MHD effects. The conductivity required to produce significant changes in the free stream flow enthalpy can be estimated from the magnetic interaction parameter,

$$I_{FS} = \frac{Lorentz\ force}{Inertia\ force} = \frac{\sigma B^2 L}{\rho U} \sim 1 \quad , \tag{1}$$

where B is the magnetic field, L is the length of the MHD channel, ρ is the flow density, and U is the free stream flow velocity. Assuming B~10 T, L~1 m, ρ~0.01-0.1 m^3 (for a room temperature flow at P~0.01-0.1 atm), and U~1000 m/s, one obtains a conductivity of σ~0.1-1.0 mho/m. Recent experimental and computational results suggest that such values of electrical conductivity in low-temperature supersonic flows can be achieved using efficient nonequilibrium ionization methods, such as high-energy electron beams or pulsed electric discharges [6,7]. The above estimate also suggests that noticeable MHD effects in cold supersonic flows can be produced only using powerful, large-scale superconducting magnets. Indeed, Eq. (1) suggests that for less powerful rare earth permanent magnets (B~1.0-1.5 T) the required conductivity increases up to σ~10-100 mho/m. However, such low-cost, relatively lightweight magnets may be usable for supersonic flow control applications that can be realized at lower values of electrical conductivity. Qualitatively, these applications might include control of turbulent transition in the supersonic ionized boundary layer and supersonic flow separation control, which both critically affect aerodynamic drag and heat transfer on a hypersonic vehicle. Indeed, in the boundary layer the appropriate characteristic velocity scale is the friction velocity,

$u^+ = \sqrt{\tau_w / \rho} = U\sqrt{c_f / 2} \approx 0.04U$. Here τ_w is the shear stress on the wall, and $c_f / 2 = \tau_w / \rho U^2 \approx 0.03 \cdot \mathrm{Re}_x^{-0.2}$ is the flat plate turbulent boundary layer skin friction coefficient [8], $c_f / 2 = 1.9 \cdot 10^{-3}$ at $\mathrm{Re}_x \sim 10^6$. Therefore, the boundary layer magnetic interaction parameter can be expressed as

$$I_{BL} = \frac{Lorentz\ force}{Inertia\ force} = \frac{\sigma B^2 L}{\rho u^+} = \frac{\sigma B^2 L}{\rho U\sqrt{c_f / 2}} \sim 1 \quad , \tag{2}$$

which has been suggested in Refs. [9-11]. Equation (2) suggests that the near-wall boundary layer flow can be affected at significantly lower conductivity values, $\sigma \sim 0.3\text{-}3.0$ mho/m, which can be achieved in nonequilibrium plasma flows.

Boundary layer transition control seems to be a particularly promising application of the MHD supersonic flow control concept, because only relatively weak actuating forces might be needed to affect the flow instability development. Thus, the delay or acceleration of the transition may be achieved by suppression or enhancement of initial instability waves at an early stage of the boundary layer flow development for the purpose of drag and heating reduction, or for the purpose of fuel mixing enhancement. Since the disturbance waves are initially very weak, their control by magnetic forces may only require relatively weak electromagnetic fields and/or fairly low electrical conductivity in the gas flow. Similar qualitative arguments can be suggested with regard to flow separation control since the flow momentum in the vicinity of the separation and reattachment points is rather low and affecting it might not require a significant Lorentz force. These arguments are consistent with results of experiments in a salt water turbulent boundary layer [9], which demonstrated possibility of both reduction and amplification of the turbulence intensity by Lorentz forces produced by permanent magnets, at a conductivity of $\sigma \sim 3$ mho/m. These results suggest the need for an experimental study of the feasibility of supersonic boundary layer control using MHD body forces.

Previously, we have detected the MHD effect in a M=4 helium nonequilibrium plasma flow with the magnetic field produced by a permanent magnet [10]. In Ref. [10], the fluctuation spectra have been measured by a microphone placed in the test section wall. However, in the presence of high-power electric discharges and strong magnetic fields diagnostics involving

microphones, pressure transducers, hot wires, etc. are subjected to significant electromagnetic interference. In many cases, electromagnetic shielding using a Faraday cage around the plasma section proves to be ineffective, and for larger scale tests appears to be impractical. Also, in Ref. [10] the flowfield in the test section (in particular, the boundary layer thickness) was not well characterized. Recently, a new nonequilibrium plasma supersonic MHD wind tunnel facility has been developed at Ohio State. It is specifically designed for studies of MHD effects on turbulent transition in the boundary layer and on the supersonic flow separation, as well as control and stability of electric discharge plasmas in MHD test sections in the presence of transverse and axial electric fields and transverse magnetic field. Recent results obtained at this facility show that it produces stable, diffuse, and uniform plasma flows in the supersonic MHD test section, with good flow quality [12-14]. The main objective of the present work is detecting the Lorentz force effect on the supersonic ionized boundary layer fluctuation spectra using optical diagnostics, which would greatly reduce electromagnetic interference from the plasma and the magnetic field.

2. Experimental

The experiments have been conducted at a new supersonic nonequilibrium plasma/MHD wind tunnel facility at the Nonequilibrium Thermodynamics Laboratories. This facility generates stable, diffuse, good flow quality supersonic flows of nonequilibrium plasmas at M=3-4 in a uniform magnetic field up to B=2 T, and can be operated continuously. Preliminary experimental results using this facility have been recently reported in Ref. [12-14]. The schematic of the experiment is shown in Fig. 1. An aerodynamically contoured M=3 supersonic nozzle made of transparent acrylic plastic is connected to a 2 cm x 4 cm rectangular cross section test section 12 cm long, and an angle step diffuser, as shown in Fig. 1. The top and bottom walls of the test section are diverging at a 0.5^{o} angle each to provide boundary layer relief. The nozzle / test section / diffuser assembly is attached to a vacuum system connected to a 1200 ft^3 dump tank pumped out by an Allis-Chalmers 1300 cfm rotary vane vacuum pump. The minimum pressure in the vacuum system sustained by the pump is 35-40 torr, which necessitates the use of a supersonic diffuser with the nozzle / test section operated at relatively low stagnation and static

pressures (P_0=1/3-1 atm, P_{test}=7-20 torr). The nozzle assembly is equipped by three pressure taps, shown in Fig. 1, measuring plenum pressure as well as static pressures at the beginning and at the end of the test section. The test section also has several Pitot ports, also shown in Fig. 1. The Pitot tube probes can be moved in and out of the flow during the experiment, which allows Pitot pressure profile measurements in both horizontal and vertical planes. The nozzle throat dimensions are 9.5 mm x 20 mm, which gives the mass flow rate through the test section of $\dot{m}$=15 g/sec at P_0=1/3 atm and $\dot{m}$=45 g/sec at P=1 atm.

Ionization in the M=3 test section is produced by a transverse RF discharge sustained between two electrode blocks 3 cm long flush mounted in the side test section walls (see Fig. 1). Each electrode block, manufactured of high-temperature machinable mica ceramic, incorporates three copper strip electrodes 35 mm long and 5 mm wide. The electrodes are rounded at the edges to prevent high electric field concentration and "hot spot" formation in the plasma near the edges. The use of dielectric (ceramic) layers between the electrodes and the flow precludes secondary ionization from the electrode surfaces, which improves the stability of the transverse RF discharge sustained in the test section [15]. The RF discharge is produced using a 5 kW, 13.56 MHz Dressler power supply with an automatic impedance matching network. In the present experiments, very good impedance matching has been achieved for RF discharge powers up to 1 kW, with only about 1-3% of the input RF power reflected back. The entire nozzle / test section / diffuser assembly was placed between the poles of a GMW water cooled electromagnet, as shown in Fig. 1. The magnet can generate a steady-state magnetic field up to B=3.5 T between two circular poles up to 25 cm in diameter. The magnetic field can be generated in two opposite directions transverse to the flow, shown as "east" and "west" in Fig. 1. In the present experiments, for the distance between the 15 cm diameter poles of 6 to 7 cm, the magnetic field at maximum current through the magnet coils of 140 A is up to B=1.7-1.8 T. For relatively short run durations (of the order of tens of seconds), the magnetic field can be significantly increased by temporarily increasing the magnet current (up to ~200 A) and chilling the cooling water.

The transverse DC electrical current (sustainer current) in the supersonic flow ionized by the RF discharge is sustained by applying a DC field (up to 500 V/cm) to two 50 mm x 20 mm DC electrode blocks flush mounted in the top and bottom nozzle walls 4 cm apart, perpendicular both to the flow velocity and to the magnetic field direction, as shown in Fig. 1. The applied DC field, which is far too low to produce additional ionization in the flow, except in the DC cathode

layer, is needed to sustain transverse (MHD) current. Both continuous and sectioned electrode blocks have been made of high-temperature aluminum silicate ceramic with electrodes made of copper. The continuous copper electrodes are 45 mm long each. The sectioned electrode blocks consist of five copper electrode strips 5 mm long each. Sectioned electrodes would allow sustaining both transverse and axial DC electric fields in the test section. However, in the present work, only transverse DC field was applied to the sectioned electrodes, which were therefore short-circuited within each DC electrode block. The DC field is applied using a DEL 2 kV / 3A power supply operated in a voltage stabilized mode, with a 0.5-5.0 kΩ ballast. From Fig. 1, it can be seen that RF ionization is produced approximately 2 cm upstream of the DC electrodes. Current in the DC sustainer circuit is measured using a Tektronix AM503S current probe.

Optical access to the flow is provided using two 1"x1/2" glass windows in the top and bottom walls of the M=3 test section (see Fig. 1). The windows are centered in the flow. Our previous Pitot tube measurements showed that the side wall boundary layer thickness in M=3, P_0=1/3-1 atm flows is 5-8 mm [12]. Therefore, the test section provides optical access approximately to one half of both side wall boundary layers. Boundary layers in the M=3 flow without plasmas are also visualized using a Z-type shlieren system with 1 kW continuous light source, 60" focal length spherical mirrors, and a high resolution COHU CCD camera.

MHD effect on a supersonic ionized boundary layer was studied using a Laser Differential Interferometry (LDI) diagnostics described in greater detail in Ref. [16]. Briefly, a plane polarized He-Ne laser beam (Coherent He-Ne laser, model # 31-2025) is split into two plane polarized beams using a quarter wave plate and a Wollaston prism (see Fig. 2) and sent through two different regions in the supersonic flow. The reference beam is passing through the flow along the centerline and the probe beam is passing through the boundary layer (see Fig. 2). The resultant phase shift between the two beams is proportional to the line-of-sight averaged density difference along the beam paths. Therefore, Fourier transform of the resultant interference signal performed by the Stanford Research Systems (Model SR 785) Dynamic Signal Analyzer yields the boundary layer density fluctuation spectrum (relative to the reference laser beam passing through the centerline of the flow). The location of the probe beam can be controlled by rotating the prism. LDI signal acquisition, averaging, and processing by the signal analyzer requires a steady state flow run time of 1-5 sec, depending on the number of averages. Typically, good signal to noise is achieved for the acquisition / processing times of 2-3 sec.

One of the main objectives of the present work was to measure the effect of the Lorentz force on the low-temperature, ionized, supersonic boundary layer, in particular on the density fluctuation spectrum. Since in the present experiments the MHD loading parameter is quite high, $K=E_y/uB_z\sim40$, the effect of Joule heat on the flow might be quite substantial, possibly exceeding the Lorentz force effect. For this reason, the LDI measurements are always performed at four sets of conditions, with the magnetic field turned on: (i) in a cold supersonic flow without plasmas, (ii) in a RF-ionized flow without DC electric field applied, i.e. when the time-averaged Lorentz force is zero, (iii) in a RF-ionized flow with DC field applied, with the Lorentz force directed downstream, and (iv) in a RF-ionized flow with DC field applied, with the Lorentz force directed upstream. The purpose of this approach was to isolate the possible MHD effect, which should depend on the Lorentz force direction, from the polarity-independent effect of Joule heat. Downstream and upstream Lorentz force was produced for both possible directions of the transverse B field by changing the polarity of the DC electric field. To evaluate run-to-run variation of the LDI spectra, several runs (2 to 4) have been conducted for each set of conditions.

3. Results and discussion

3.1. Flow field characterization

Figure 3 shows the results of the Pitot pressure measurements in M=3 air flows at three different stagnation pressures, P_0=250 torr, P_0=500 torr, and P_0=725 torr, at the downstream end of the test section (20 cm from the nozzle throat, or 2 cm upstream of the diffuser). It can be seen that in all three cases the Pitot pressure distribution in the vertical plane is nearly uniform over about 80% of the flow (i.e. up to 16 mm distance from the centerline). In the horizontal plane, the Pitot tube remains uniform over about 50% of the test section at P_0=250 torr and over about 35% of the test section at P_0=500 torr. In these two cases, the centerline Pitot pressures correspond to Mach numbers of M=2.88 and M=2.84, respectively. This is consistent with Mach numbers inferred from the static pressure measurements at the end of the test section, P=9.3 torr, M=2.79 at P_0=250 torr, and P=19.5 torr, M=2.76 at P_0=500 torr. The increase of the side wall boundary layer thickness with pressure is consistent with 3-D compressible Navier-Stokes

turbulent flow calculations [17] and may possibly be an indication of boundary layer transition over the range of Reynolds numbers tested.

Fig. 4 shows additional Pitot tube measurements in three horizontal planes at P_0=250 torr, (A) at the centerline plane, (B) 10 mm above the centerline plane, and (C) 10 mm below the centerline plane. It can be seen that the Pitot pressure distribution across the centerline plane (location A) indicates a thicker boundary layer compared to the other two planes (B and C). In other words, these measurements suggest the presence of a bulge in the side walls boundary layers near the centerline plane, which may be due to a secondary cross flow present in the rectangular cross section test section [18].

Figure 5 shows a schlieren image of the flow in the test section (20 cm from the nozzle throat, or 2 cm upstream of the diffuser, looking top to bottom), at stagnation pressure of P_0=250 torr. The light areas on both sides of the flow are boundary layer regions. It can be seen that the size of the core flow is approximately 30% of the distance between the side walls of the test section, which is consistent with the Pitot probe measurements (see Fig. 4).

3.2. Electrical measurements

Figure 6 shows a photograph of transverse 500 W RF discharge in the M=3 flow of nitrogen at the plenum pressure of P_0=318 torr (P_{test}=11.6 torr), with the test section mounted to the vacuum flange outside the magnet. At these conditions, the RMS RF voltage and current are I_{RMS}=1.6 A and U_{RMS}=3.7 kV, respectively. It can be seen that the diffuse discharge occupies nearly the entire region between the RF blocks. The RF plasma glow is more intense in the center of the flow (because of a stronger electric field near the center of the electrode assembly) and near the top and bottom test section walls (because of a longer flow residence time and lower density in the boundary layers, which may result in preferential ionization there). The RF afterglow plasma is quite long (at least 20 cm) and is extending into the diffuser, where it visualizes the oblique shock pattern (see Fig. 6). The plasma flow visualization of shock waves, boundary layers, and wakes, also observed in our previous experiments [19-21], can be used to study the possible MHD effect on the supersonic flow separation.

Figure 7 shows a photograph of crossed transverse discharges (RF + DC) sustained in a supersonic flow of nitrogen (M=3, P_0=270 torr), in the presence of transverse magnetic field of

B=1.5 T. The flow is photographed at a sharp oblique angle from the nozzle plenum side. The RF discharge power is 500 W, and the DC power supply voltage is U_{PS}=1500 V (with a 5.2 kΩ ballast resistor in series with the discharge electrodes). It can be seen that the plasma in the MHD test section is diffuse, filling essentially the entire volume between the electrodes. A bright region near the bottom of the flow may be due to preferential ionization in the bottom wall boundary layer, as also suggested by Fig. 6. At these conditions, the measured DC sustainer current is I_y=128 mA. It was also found that increasing the magnetic field in the range B=0 to 1.5 T considerably improves the plasma stability and makes it more uniform and diffuse. Figure 8 shows the results of the time-resolved current and voltage measurement in the DC circuit for the conditions of Fig. 7. Voltage and current oscillations are due to the RF current leakage into the DC circuit. Note that the time-averaged Lorentz force applied to the flow is determined by the time-averaged DC current, which in this measurement was I_y=115 mA.

Figure 9 shows results of time-averaged transverse DC current measurements in M=3 flows of an 80% N_2 – 20% He mixture and pure nitrogen as functions of the applied magnetic field. In these measurements, plenum pressure was P_0=270 torr (test section static pressure P=12 torr), RF power was 200 W, DC power supply voltage U_{PS}=1400 V, and the ballast resistance was R=5.2 kΩ. It can be seen that with all other conditions being the same, the current decreases with the magnetic field. This is the result of the Hall effect, which in the absence of the axial electric field reduces the transverse current component, I_y, and generates the axial current, I_x, [22],

$$I_y = \frac{\sigma}{1+\beta^2}(E_y - uB_z)A \quad , \quad I_x = \beta\frac{\sigma}{1+\beta^2}(E_y - uB_z)A \quad , \tag{3}$$

In Eqs. (3), σ is the scalar electric conductivity, A=10 cm^2 is the total surface area of the DC electrodes, and $\beta = {eB_z}/{m_e\nu_{en}}$ is the Hall parameter, i.e. the ratio of the electron cyclotron frequency, eB_z/m_e, to the electron-neutral collision frequency, ν_{en}. Note that the factor uB_z in Eqs. (3) can be neglected compared to the transverse electric field, E_y, because of high values of the MHD loading parameter, $K=E_y/uB_z$~40, under the present conditions. Transverse electric field in Eqs. (3) is estimated as $E_y \cong (U_{PS} - I_yR)/h$, where h=4 cm is the test section height. Assuming that

the scalar electric conductivity, σ, is independent of the magnetic field, the results shown in Fig. 9 can be used to infer the values of the effective Hall parameter at these conditions, using the first of Eqs. (3). The results, plotted in Fig. 10, show that the Hall parameter reaches $\beta \approx 3$ at B=1.4 T. This is also consistent with the theoretical value of the Hall parameter for the electron collision frequency in nitrogen at $N=7.5 \cdot 10^{17}$ cm^{-3} and $E_y/N=(U_{PS}-IR)/h/N=(2-4) \cdot 10^{-16}$ V·cm^2, calculated from the solution of Boltzmann equation for plasma electrons at these conditions, $\nu_{coll}=(0.9-1.1) \cdot 10^{11}$ s^{-1}, $\beta=2.4-2.9$ at B=1.5 T [3].

Figure 11 shows the results of the transverse DC current measurements in M=3 nitrogen flows as a function of the RF discharge power, at two values of magnetic field, B=1.0 T and B=1.4 T. In these measurements, again both the DC power supply voltage and the ballast resistance were kept the same, $U_{PS}=1400$ V and R=5.2 kΩ. It can be seen that the current increases with the RF power, up to $I_y=100-150$ mA at 500 W, which is due to the increased conductivity of the plasma in the RF discharge. Since the dependence of the effective Hall parameters on the magnetic field (at the same conductivity) has already been determined from the results of Fig. 10, the data of Fig. 11 can now be used to infer the electric conductivity of the flow in the MHD test section at these conditions (at the same magnetic field), using the first Eq. (3). The results are summarized in Fig. 12. One can see that the conductivity considerably increases with the RF power, up to $\sigma=0.05$ mho/m. Extrapolating these results to the RF power of ~1 kW, easily attainable at the present MHD facility, gives $\sigma \sim 0.1$ mho/m. Note that the present procedure for calculating the conductivity neglects the DC cathode voltage drop, which results in an underestimated conductivity value. Assuming normal current density in the cathode layer, the voltage drop for copper cathode in a nitrogen glow discharge plasma at $N \sim 10^{18}$ cm^{-3} is $U_{cathode} \sim 100-150$ V [15]. At the present conditions, this produces up to 25% uncertainty in the flow conductivity.

As shown in our recent experiments [23], further conductivity increase, without significantly raising the ionization source power, can be achieved by replacing the sine wave RF plasma generator with a repetitively pulsed (up to 50 kHz), short pulse duration (10-20 ns), high voltage (20-30 kV) power supply. Nonequilibrium plasma generated by such pulsed power sources has a much larger fraction of the input power going to ionization [15], which considerably increases the plasma conductivity at a comparable discharge power budget. The short pulse duration and a very low duty cycle, ~1/1000, also preclude plasma instability

development, which greatly improves stability of these plasmas at high currents. Therefore, the use of the repetitively pulsed ionization is expected to produce a more pronounced Lorentz force effect on the flow.

It appears that electrical conductivity of σ=0.05 mho/m should make possible sustaining rather high DC currents in the MHD test section, on condition that the Hall effect is mitigated (i.e. in the Faraday configuration). Indeed, from the data of Figs. 11,12, at B=1.4 T and $U_y=U_{PS}-I_yR\sim800$ V (transverse field of $E_y\sim200$ V/cm), the transverse current should be $I_y\sim1$ A. However, the actual conductivity and current values for this electrode configuration are lower by a factor $(1+\beta^2)\cong10$, i.e. by an order of magnitude (see Fig. 11). Transverse current reduction due to the Hall effect can be mitigated by applying an axial electric field E_x in order to cancel the axial current J_x (see Eqs. (3)). This can be achieved by individually ballasting the sectioned MHD electrodes (see Fig. 1). However, due to the small MHD channel length-to-height ratio of only 5 cm / 4 cm = 1.25, the axial electric field in this case may be limited to the near-electrode areas and may be rather weak far from the MHD electrodes, i.e. in the core flow.

3.3. LDI measurements

Figure 13 shows the LDI spectra taken in a M=3 nitrogen flow at the baseline plenum pressure of P_0=250 torr, i.e. at the conditions of Fig. 5. The probe laser beam is located midway between the wall and the centerline, as shown in Fig. 5. The two groups of spectra shown in Fig. 13 are both measured in the presence of B=1.5 magnetic field (i) in the flow without plasmas, and (ii) in the RF-ionized flow without the DC field applied. In both these cases, there is no net Lorentz force applied to the flow, while in case (ii) there is Joule heating of the flow by the 500 W RF discharge. Typically, the raw LDI spectra have a run-to-run intensity variation of up to 1-2 dB, which is most likely due to the effect of magnetic field on the mirror holder assembly mounting the mirrors to the magnet frame, which affects the LDI beam alignment. Therefore, in the present work the raw LDI spectra have been normalized (i.e. shifted up or down on a log-log scale) to match their intensities at the same conditions. Note that such intensity normalization did not affect the shape of the spectra. From Fig. 13, which shows two spectra for each set of conditions, it can be seen that the shape of the intensity-matched spectra has a very good run-to-run reproducibility, typically within 0.5-1.0 dB. Also, the results of Fig. 13 show that the cold

flow spectra and the RF-ionized flow spectra (without the DC field applied) are very nearly identical. This suggests that the effect of Joule heating on the boundary layer density fluctuations at these conditions is small.

Note that the shape of the LDI spectra, i.e. a nearly flat plateau followed by a roll-off is qualitatively consistent with the in-flight supersonic boundary layer measurement [24], shown in Fig. 14. In the present measurements, the roll-off begins at the dimensionless frequency of $\omega^*=\omega\delta/U_0 \sim 2\pi \cdot 40$ kHz $\cdot$ 0.5 cm / 600 m/s ~ 2, which is again consistent with the results of Ref. [24].

Figure 15 shows the LDI spectra at the same flow conditions, for sets (iii) and (iv), i.e. in a RF-ionized flow with DC field applied, for the accelerating Lorentz force, and in a RF-ionized flow with DC field applied, for the decelerating Lorentz force (several runs are shown for each set). Note that in this series of experiments, both accelerating and decelerating Lorentz force within each set have been produced for two opposite directions of the magnetic field (B=1.5 T) by changing the DC voltage polarity (U_{PS}=1500 V, ballast resistor 1 kΩ). Again, one can see that reproducibility of the shape of the spectra for each set is very good, below 1 dB. It can also be seen that Fig. 15 shows small (~2 dB) but consistently reproduced difference between the spectra for the accelerating (set (iii)) and decelerating (set (iv)) Lorentz force. In particular, the fluctuation intensity in the entire plateau from 2 kHz to 40 kHz is higher in the flow with the decelerating Lorentz force. This is consistent with the results obtained in the salt water boundary layer [9], where decelerating Lorentz force was shown to amplify turbulent fluctuations while accelerating force reduced them. Also, in the present experiments the fluctuation intensity increase has been observed for both possible B and E field configurations giving the same upstream Lorentz force direction, which suggests this to be a true MHD effect.

Figure 16 and 17 both show the LDI spectra for the accelerating and decelerating Lorentz force, at the same conditions as in Fig. 15, but at higher RF discharge powers, 0.75 kW (Fig. 16) and 1 kW (Fig. 17). For both series of experiments, the results of two runs are shown for every set of conditions, to demonstrate good run-to-run reproducibility. One can see that the effect of density fluctuation increase in the presence of decelerating Lorentz force is detected for both magnetic field directions ("east" and "west", as shown in Fig. 1), again with good run-to-run reproducibility. It can be seen that in the region from about 15 kHz to 50 kHz the fluctuation intensity for the decelerating Lorentz force is higher by about 1 dB at RF power of 0.75 kW (see

Fig. 16), and by about 2 dB at the RF power of 1 kW (see Fig. 17). Note that when the RF power is increases from 0.75 kW to 1 kW (i.e. by 33%), the transverse DC current increases by about 10-15%, from 180-200 mA to 200-230 mA, depending on the B field and DC electric field polarity. Finally, Fig. 18 shows the spectra of Fig. 17 plotted in linear scale, to better illustrate the MHD effect on density fluctuations. From Fig. 18, it can be seen that the fluctuation intensity in the frequency range of 15-50 kHz increases by up to 20%.

To summarize, the results of Figs. 13, 15-18 consistently show the well-reproduced amplifying effect of decelerating Lorentz force on the boundary layer density fluctuations, which increases with the flow conductivity and is not related to Joule heating. However, additional experiments are needed to determine whether MHD forcing directly affects density fluctuations in the ionized flow, or the effect is indirect, such as Lorentz force modification of the secondary cross flow in the sidewall boundary layer.

4. Summary

The new blowdown nonequilibrium plasma MHD supersonic wind tunnel operated at complete steady state has been developed and tested. The wind tunnel can be operated at Mach numbers up to M=3-4, at mass flow rates of up to $\dot{m}$=45 g/sec at P_0=1 atm. Pitot tube and schlieren measurements in a M=3 test section showed reasonably good flow quality, up to 80% inviscid core across the larger dimension and up to 50% inviscid core across the smaller dimension of the flow. Stable and diffuse transverse RF discharges (RF power up to 1 kW) have been sustained in M=3 nitrogen flows, at magnetic fields of up to B=1.5 T. Operation at higher magnetic fields results in a more uniform RF plasma in the MHD test section. Hall parameter and electric conductivity of the flow have been inferred from the DC (MHD) current and voltage measurements at different values of the magnetic field. At B=1.5 T and RF power of 500 W, the Hall parameter is $\beta \cong 3$ and the conductivity is $\sigma \cong 0.05$ mho/m. At the RF power of 1 kW, the extrapolated conductivity is ~0.1 mho/m.

The results of the present work demonstrate the Lorentz force effect on the supersonic boundary layer in M=3 flows of nitrogen ionized by a high-power transverse RF discharge in the presence of the magnetic field. Boundary layer density fluctuation spectra are measured using the

Laser Differential Interferometry (LDI) diagnostics. In particular, decelerating Lorentz force applied to the flow produces a well reproduced increase of the density fluctuation intensity by up to 10-20% (1-2 dB), compared to the accelerating force of the same magnitude applied to the same flow. The effect is produced for two possible combinations of the magnetic field and current directions producing the same Lorentz force direction (both for accelerating and decelerating force). The effect is observed to increase with the flow conductivity. On the other hand, the effect of Joule heating on the fluctuation spectra appears insignificant.

Further experiments to characterize the flow field in the test section, in particular, to determine the state of the boundary layer are currently underway.

6. References

1. Fraishtadt, V.L., Kuranov, A.L., and Sheikin, E.G. "Use of MHD Systems in Hypersonic Aircraft," Technical Physics, Vol. 43, No. 11, 1998, pp. 1309-1314
2. Kuranov, A.L., and Sheikin, E.G., "Magnetohydrodynamic Control on Hypersonic Aircraft Under "Ajax" Concept", Journal of Spacecraft and Rockets", Vol. 40, No. 2, 2003, pp. 174-182
3. Adamovich, I.V., Rich, J.W., and Nelson, G.L. "Feasibility Study of Magneto-hydrodynamics Acceleration of Unseeded and Seeded Air Flows", AIAA Journal, Vol. 36, No. 4, 1998, pp. 590-597
4. Macheret, S.O., Shneider, M.N., and Miles, R.B., "Magnetohydrodynamic Control of Hypesonic Flow and Scramjet Inlets Using Electron Beam Ionization", AIAA Journal, Vol. 40, No.1, 2002, pp. 74-81
5. Park, C., Mehta, U.B., and Bogdanoff, D. W., "Magnetohydrodynamic Energy Bypass Scramjet Performance with Real Gas Effects", Journal of Propulsion and Power, Vol. 17, No. 5, 2001, pp. 1049-1057
6. Macheret, S.O., Shneider, M.N., Miles, R.B., and Lipinski, R.J., "Electron Beam Generated Plasmas in Hypersonic MHD Channels", AIAA Journal, Vol. 39, No.6, 2001, pp. 1127-1136
7. Macheret, S.O., Shneider, M.N., and Miles, R.B., "MHD Power Extraction from Cold Hypersonic Air Flow with External Ionizers", Journal of Propulsion and Power, Vol. 18, No.

2, 2002, pp. 424-431

8. Schlichting, H., "Boundary Layer Theory", McGraw-Hill, New York, 1968, Chap. XXI
9. Henoch, C. and Stace, J., "Experimental Investigation of a Salt Water Turbulent Boundary Layer Modified by an Applied Streamwise Magnetohydrodynamic Body Force," Physics of Fluids, Vol. 7, No. 6, 1995, pp. 1371-1383
10. Palm, P., Meyer, R., Ploenjes, E., Bezant, A., Adamovich, I.V., Rich, J.W., and Gogineni, S., "MHD Effect on a Supersonic Weakly Ionized Flow", AIAA Paper 2002-2246, 33rd Plasmadynamics and Lasers Conference, Maui, HW, 20-23 May 2002
11. Macheret, S. O., Shneider, M. N., and Miles, R. B., "Magnetohydrodynamic and Electrohydrodynamic Control of Hypersonic Flows of Weakly Ionized Plasmas, AIAA paper 2002-2249, 33rd Plasmadynamics and Lasers Conference, Maui, HW, 20-23 May 2002
12. Meyer, R., McEldowney, B., Chintala, N., Palm, P., and Adamovich, I.V., "Experimental Studies of Plasma Assisted Ignition and MHD Supersonic Flow Control", AIAA Paper 2003-0873, 41th Aerospace Sciences Meeting and Exhibit, January 2003, Reno, NV
13. McEldowney, B., Meyer, R., Chintala, N., and Adamovich, I.V., "Measurements of Electrical Parameters of a Supersonic Nonequilibrium MHD Channel", AIAA Paper 2003-4279, 34th Plasmadynamics and Lasers Conference, Orlando, FL, 23-26 June 2003
14. Meyer, R., Chintala, N., Bystricky, B., Hicks, A., Cundy, M., Lempert, W.R., and Adamovich, I.V., "Lorentz Force Effect on a Supersonic Ionized Boundary Layer", AIAA Paper 2004-0510, 42nd Aerospace Sciences Meeting and Exhibit, January 2004, Reno, NV
15. Raizer, Yu.P., "Gas Discharge Physics", Springer-Verlag, Berlin, 1991
16. Salyer, T. R., Collicott, S. H., and Schneider, S. P., "Feedback Stabilized Laser Differential Interferometry for Supersonic Blunt Body Receptivity Experiments," AIAA-2000-0846, 38th AIAA Aerospace Sciences Meeting and Exhibit, Reno, NV, January 10-13, 2000
17. R.J. McMullan, M.F. Lindsey, I.V. Adamovich, and M. Nishihara, "Experimental Validation of a 3-D Magnetogasdynamic Compressible Navier-Stokes Solver", AIAA Paper 2004-2269, presented at 35th Plasmadynamics and Lasers Conference, Portland, OR, 29 June – 1 July 2004
18. Zhong, X., and Singh, V., "Numerical Simulation of Supersonic Boundary Layer Stability with Applied Electromagnetic Field in a Weakly Ionized Flow", AIAA Paper 2004-2724, 35th Plasmadynamics and Lasers Conference, Portland, OR, 28 June - 1 July 2004

19. Yano. R., Contini, V., Ploenjes, E., Palm, P., Merriman, S., Aithal, S., Adamovich, I., Lempert. W., Subramaniam. V., and Rich, J.W., "Supersonic Nonequilibrium Plasma Wind Tunnel Measurements of Shock Modification and Flow Visualization", AIAA Journal, vol. 38, No. 10, 2000, pp. 1879-1888
20. Merriman, S., Ploenjes, E., Palm, P., and Adamovich, I.V., "Shock Wave Control by Nonequilibrium Plasmas in Cold Supersonic Gas Flows" , AIAA Journal, Vol. 39, No. 8, 2001, pp. 1547-1552
21. Meyer, R., Palm, P., Plonjes, E., Rich, J.W., Adamovich, I.V., "The Effect of a Nonequilibrium RF Discharge Plasma on a Conical Shock Wave in a M=2.5 Flow", AIAA Journal, Vol. 41, No. 5, 2003, pp. 465-469
22. Rosa, R.J., "Magnetohydrodynamic Energy Conversion", New York, McGraw-Hill, 1968
23. Nishihara, M., Meyer, R., Cundy, M., Lempert, W.R., and Adamovich, I.V., "Development and Operation of a Supersonic Nonequilibrium MHD Channel", AIAA Paper 2004-2441, 35th Plasmadynamics and Lasers Conference, Portland, OR, 28 June - 1 July 2004
24. Belcher, P.M., "Predictions of Boundary Layer Turbulence Spectra and Correlations for Supersonic Flight", 8 Congres International D'Acoustique, Liege, 7-14 September 1965

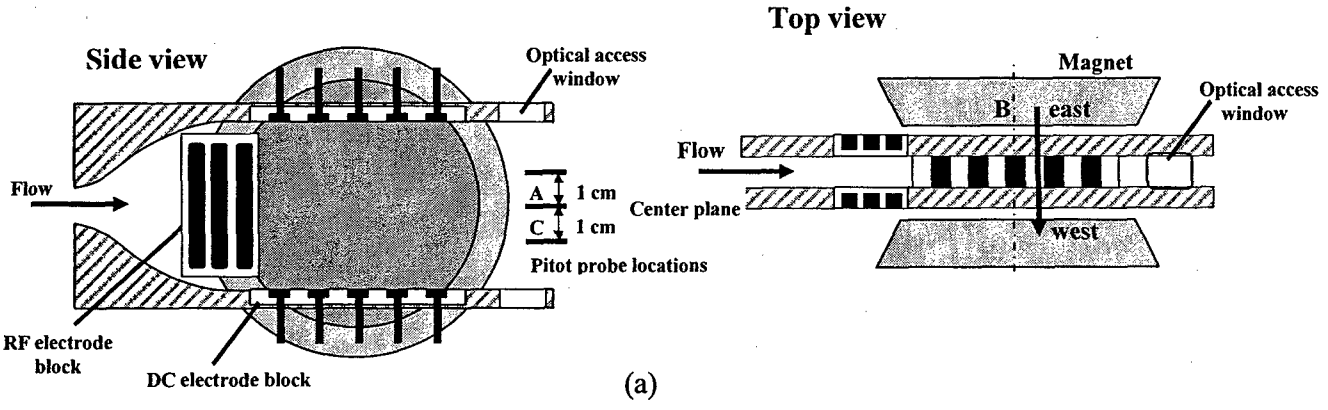

Figure 1. Schematic (a) and photographs (b, c) of a M=3 nozzle / test section / diffuser. Ionization is produced upstream of the MHD section. Locations of static pressure taps (b) and Pitot ports (c) are shown by arrows

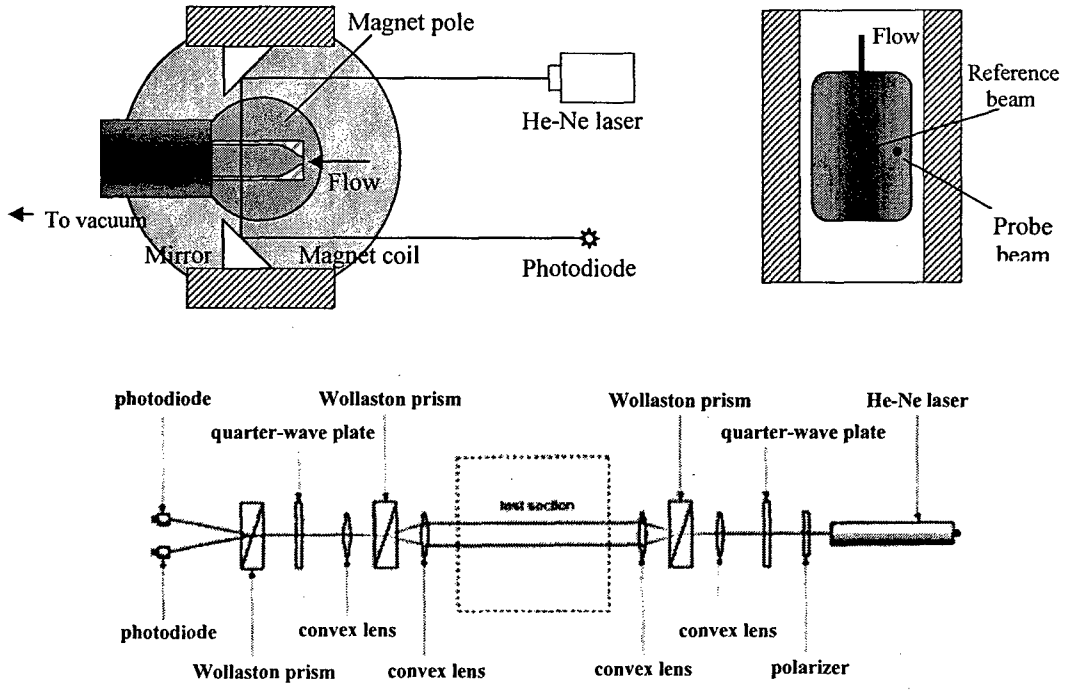

Figure 2. Layout and schematic of the LDI diagnostics

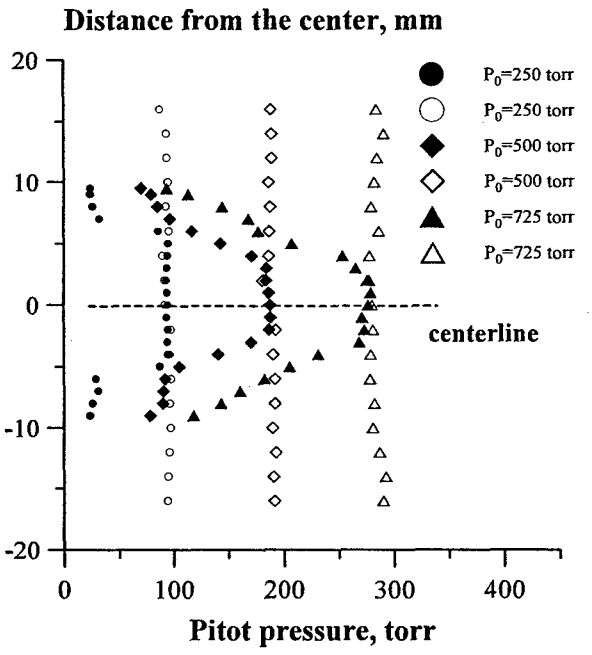

Figure 3. Summary of Pitot pressure measurements in horizontal and vertical centerline planes, at different stagnation pressures. Air, M=3. Closed symbols, horizontal plane; open symbols, vertical plane.

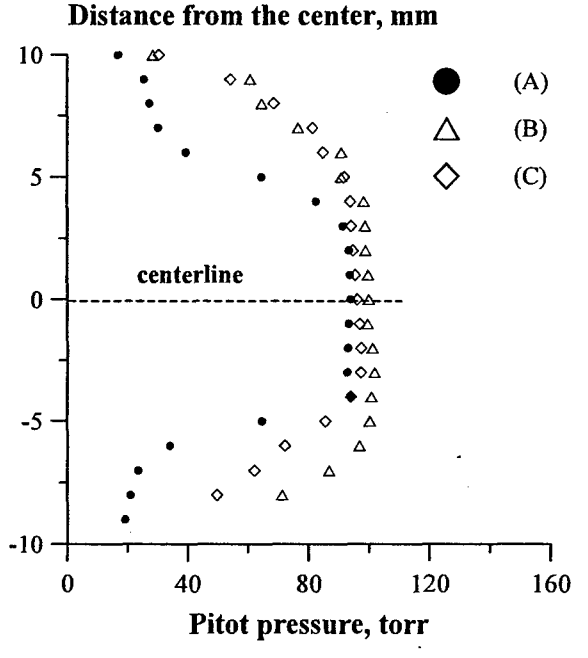

Figure 4. Pitot pressure measurements in the horizontal centerline plane (A), 10 mm above the centerline plane (B), and 10 mm below the centerline plane (C), at stagnation pressure of P_0=250 torr. Air, M=3.

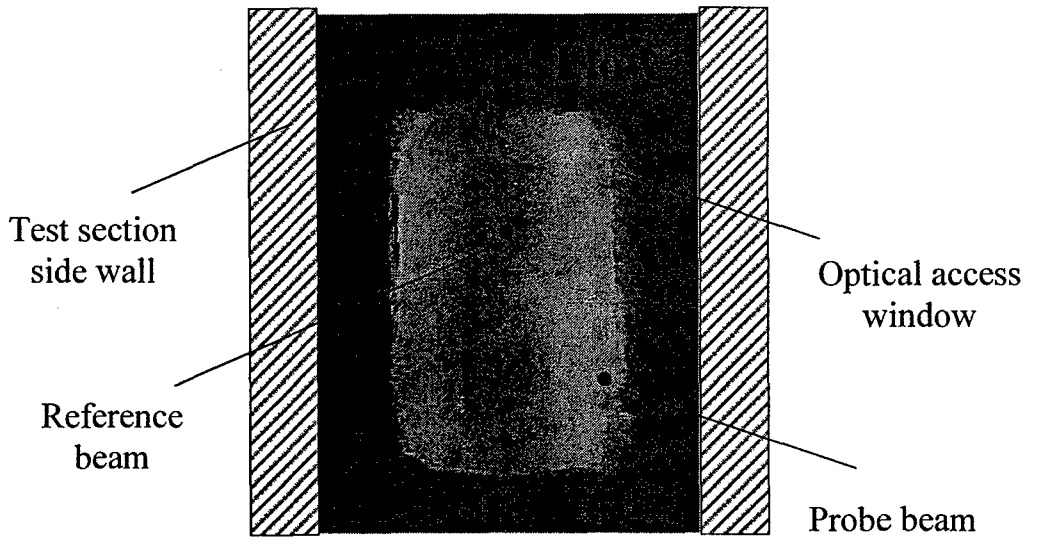

Figure 5. Schlieren image of the M=3 flow in nitrogen (P_0=250 torr, no plasmas), with the schematic of the LDI laser beam arrangement in the flow. Lighter boundary layer regions on both sides are clearly visible.

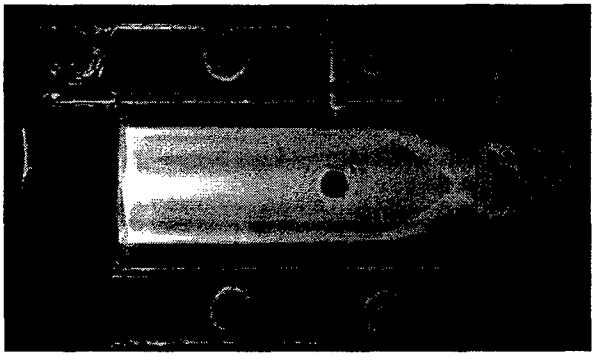

Figure 6. 500 W RF discharge in a M=3 flows of nitrogen (P_0=318 torr, P_{test}=11.6 torr, I_{RMS}=1.6 A, U_{RMS}=3.7 kV). The flow is left to right. Oblique shock train in the diffuser is clearly visible.

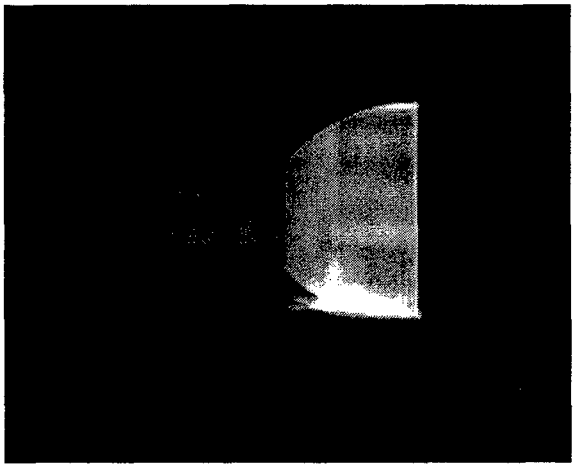

Figure 7. Photograph of a crossed discharge (RF+DC) in a M=3 nitrogen flow in magnetic field: nitrogen, P_0=270 torr, RF power 500 W, DC voltage U_{PS}=1500 V, B=1.5 Tesla, I_{DC}=128 mA. Flow is left to right.

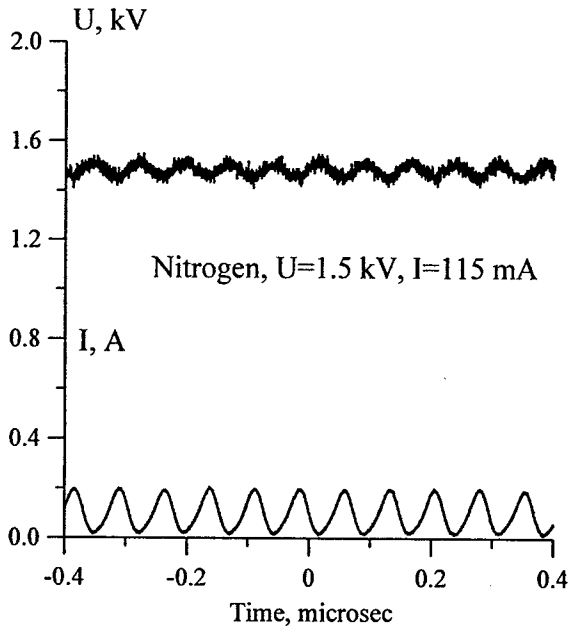

Figure 8. Current and voltage in crossed discharges (RF+DC) in the magnetic field (B=1.5 T): nitrogen, P_0=270 torr, P_{test}=15 torr, RF power 500 W, U_{PS}=1500 V, I_{DC}=115 mA

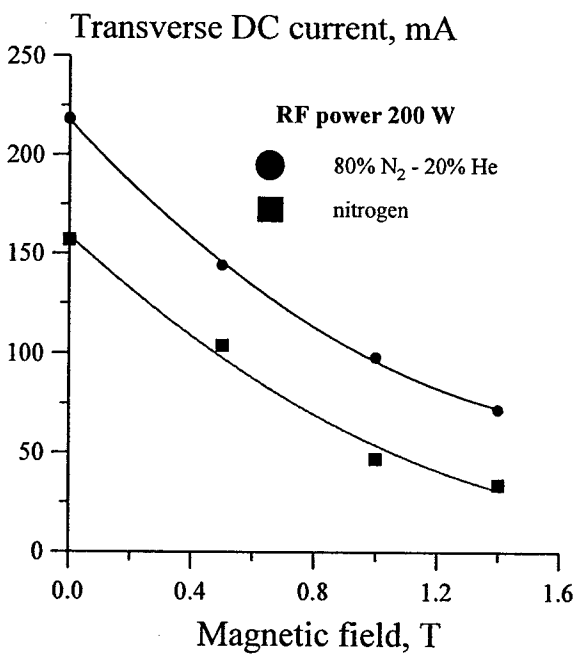

Figure 9. Transverse DC current in M=3 flows of a N_2-He mixture and nitrogen as functions of the magnetic field. P_0=270 torr, RF power 200 W, DC power supply voltage U_{PS}=1400 V.

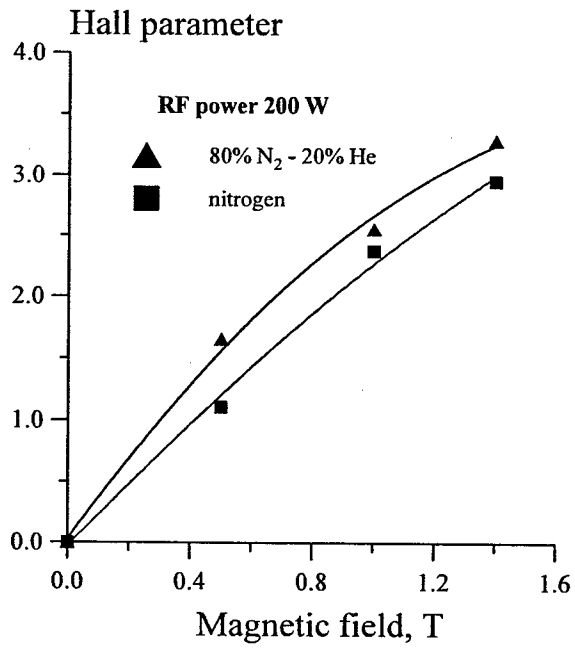

Figure 10. Hall parameters in M=3 flows of a N_2-He mixture and nitrogen as functions of the magnetic filed for the conditions of Figure 9.

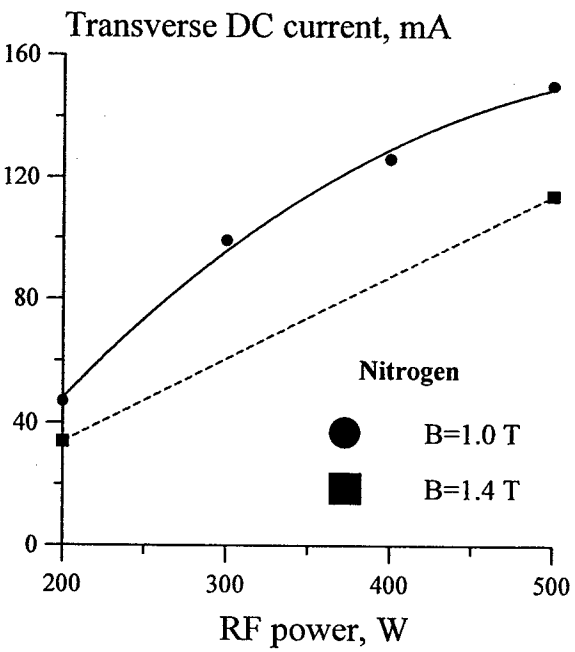

Figure 11. Transverse DC current in M=3 flows of nitrogen as functions of the RF discharge power. P_0=270 torr, DC power supply voltage U_{PS}=1400 V.

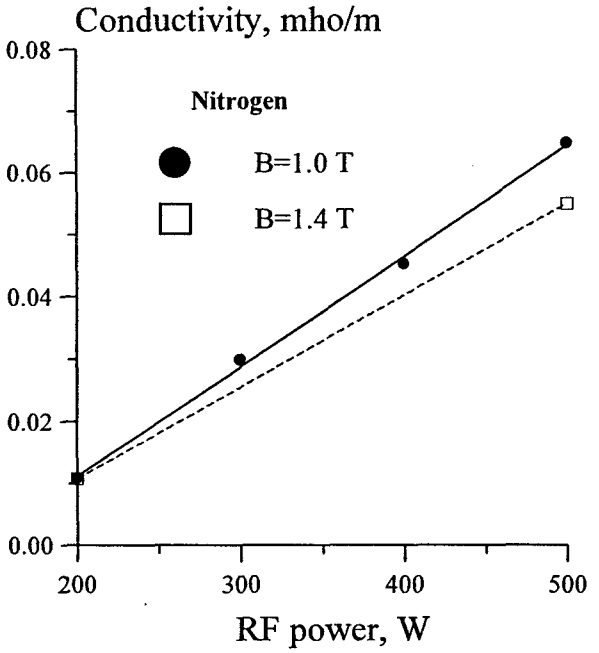

Figure 12. Electric conductivity of M=3 flows of nitrogen as a function of the RF discharge power for the conditions of Figure 11.

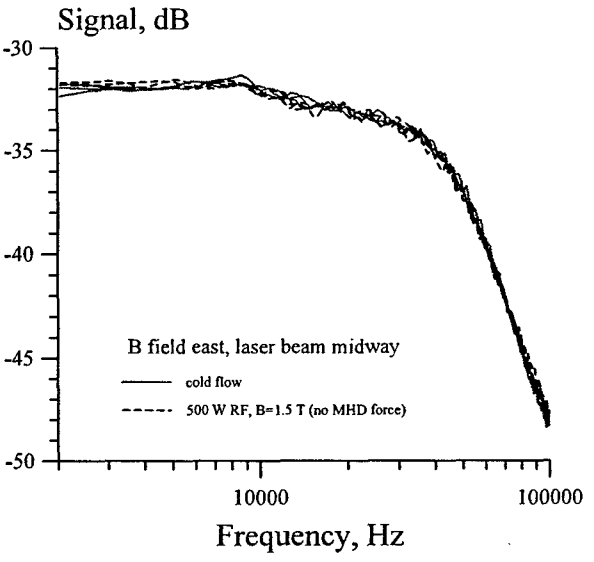

Figure 13. Overlapped LDI spectra in M=3 flows of nitrogen (P_0=250 torr, B=1.5 T, RF power 500 W), for the cold flow without plasmas and for the RF-ionized flow. No DC field and Lorentz force applied.

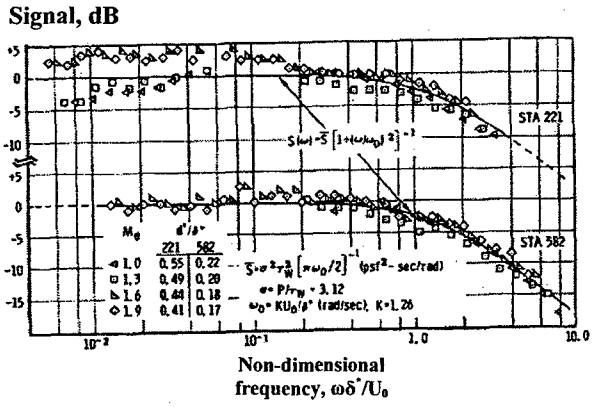

Figure 14. Pressure fluctuation spectra in a supersonic boundary layer at M=1.0-1.9. Flight measurements at 221 in. (top curve) and 582 in. (bottom curve) aft from the nose of a flight vehicle [24]

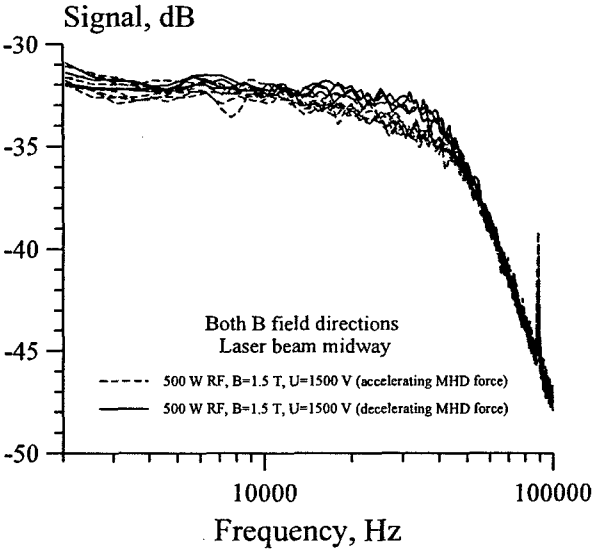

Figure 15. Overlapped LDI spectra in M=3 flows of nitrogen (P_0=250 torr, B=1.5 T, RF power 500 W, U_{DC}=1500 V), for the downstream Lorentz force (6 runs) and the upstream Lorentz force (4 runs). In both cases, the Lorentz force is produced for two opposite directions of the B field by flipping the DC electric field.

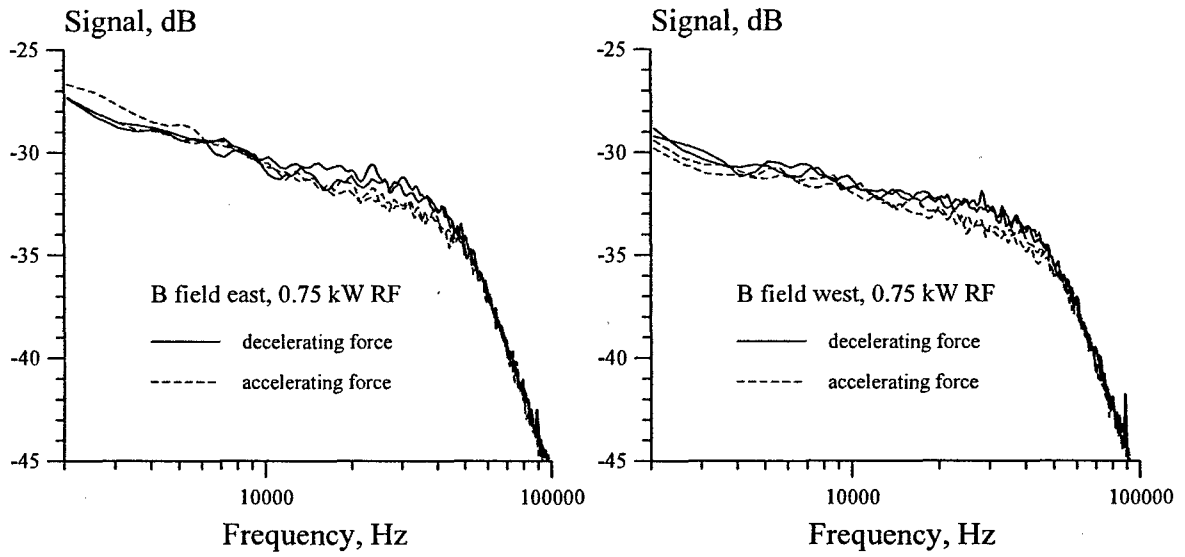

Figure 16. LDI spectra in M=3 flows of nitrogen (P_0=250 torr, B=1.5 T, RF power 0.75 kW) for two different B field and Lorentz force directions (accelerating and decelerating). For all sets of conditions, the results of two runs are shown.

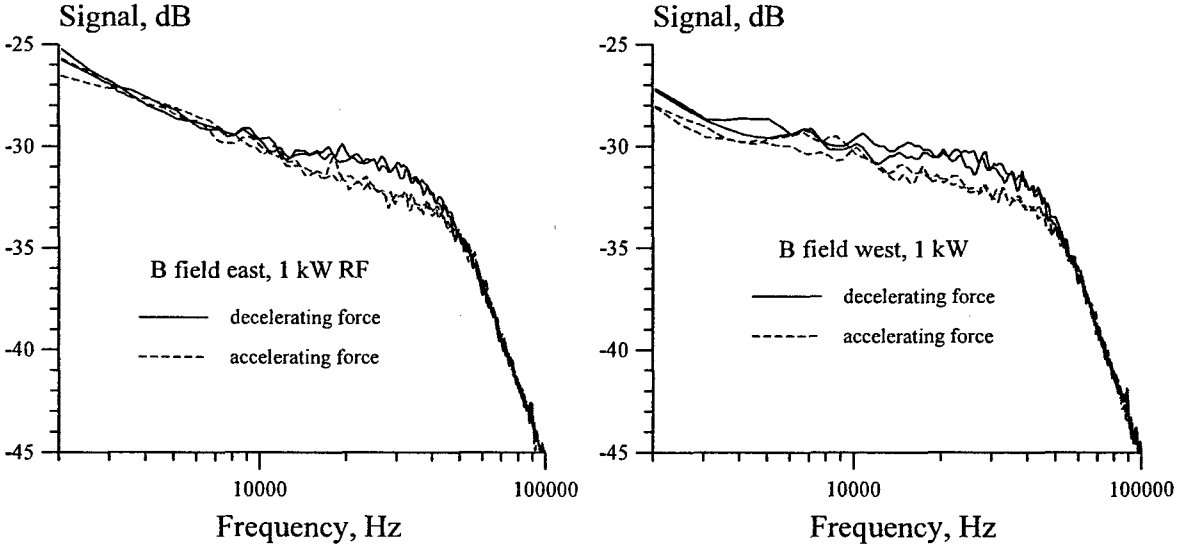

Figure 17. LDI spectra in M=3 flows of nitrogen (P_0=250 torr, B=1.5 T, RF power 1 kW) for two different B field and Lorentz force directions (accelerating and decelerating). For all sets of conditions, the results of two runs are shown.

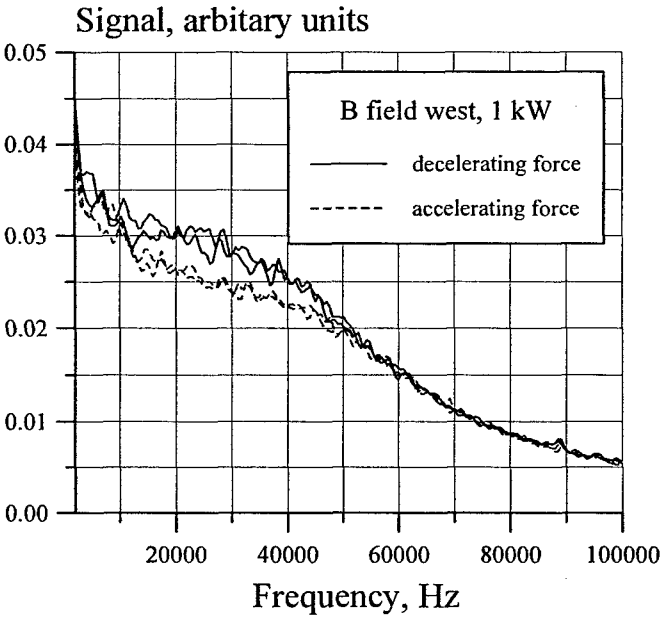

Figure 18. Linear scale LDI spectra in M=3 flows of nitrogen (P_0=250 torr, B=1.5 T, RF power 1 kW) for two different Lorentz force directions. For both sets of conditions, the results of two runs are shown. Density fluctuation increase for the decelerating force is about 20%.

CHAPTER II. SUPERSONIC NONEQUILIBRIUM BOUNDARY LAYER CONTROL USING REPETITIVELY PULSED MHD FORCING

1. Introduction

The use of nonequilibrium (low-temperature) magnetohydrodynamics for supersonic flow control, supersonic air-breathing propulsion, on-board power generation, and for development of novel hypersonic ground testing facilities continues to attract considerable interest [1-9]. Control of boundary layer transition seems to be a particularly promising application of the MHD supersonic flow control technology, because a relatively weak actuating Lorentz force may be sufficient to affect the flow field in the ionized boundary layer. Indeed, the MHD interaction parameter (i.e. the ratio of the Lorentz force work to the kinetic energy of the flow) for the free stream flow is

$$I_{FS} = \frac{\sigma B^2 L}{\rho u_\infty} \quad , \tag{1}$$

where σ is the electric conductivity, B is the magnetic field, L is the length scale, ρ is the flow density, and u_∞ is the free stream flow velocity. From Eq. (1), it can be seen that for B~3 T, L~0.1 m, u_∞~1000 m/sec, and conductivity of σ~0.1 mho/m (currently achieved in nonequilibrium supersonic flow plasmas [9]), the MHD interaction can be significant only at very low densities, $\rho \sim 10^{-4}$ kg/cm^3 (P~0.1 torr for near room temperature flows). On the other hand, for the boundary layer flow the interaction parameter can be expressed as follows [10]

$$I_{BL} = \frac{\sigma B^2 L}{\rho u^+} = \frac{\sigma B^2 L}{\rho u_\infty} \sqrt{\frac{2}{c_f}} \quad , \tag{2}$$

In Eq. (2), $u^+ = u_\infty \sqrt{c_f/2}$ is the friction velocity, and $c_f/2 \approx 0.03 \cdot \mathrm{Re}_x^{-0.2}$ is the flat plate turbulent boundary layer skin friction coefficient [11], $c_f/2 \sim 10^{-3}$ at $\mathrm{Re}_x \sim 10^7$, so that MHD interaction may become significant at significantly higher densities, $\rho \sim 3 \cdot 10^{-3}$ kg/cm^3 (i.e. at static

pressures of a few torr). Qualitatively, the delay or acceleration of the weakly ionized boundary layer transition may be achieved by suppression or enhancement of flow instabilities by MHD forcing. This method of boundary layer control can be used in cold supersonic flows for the purpose of drag and heat transfer leverage, or for the purpose of mixing enhancement.

The above estimates are consistent with successful boundary layer density fluctuation control experiments in both low-speed salt water flows (conductivity up to σ=3 mho/m, B=0.4 T, L=0.25 m, u_∞=1-5 m/sec, ρ=1 kg/cm^3, $c_f/2 \sim 10^{-3}$) [12] and in M=3 boundary layer flows weakly ionized by an RF discharge (σ~0.1 mho/m, u_∞=500 m/sec, B=1.5 T, L=0.05 m, P~10 torr, $c_f/2 \sim 10^{-3}$) [9,13,14]. In particular, recent experiments at Ohio State [9,13,14] detected an MHD effect on the level of density fluctuations in a supersonic boundary layer weakly ionized by a transverse RF discharge. In these experiments, retarding Lorentz force applied to the flow produced a well-reproduced increase of the density fluctuation intensity by up to 10-20% (1-2 dB), compared to the accelerating force applied to the same flow. On the other hand, the effect of Joule heating on the fluctuation spectra was insignificant. The effect was produced for two possible combinations of the magnetic field and current directions producing the same Lorentz force direction (both for accelerating and decelerating force). Finally, the effect was observed to increase with the RF discharge power, i.e. with the flow conductivity. Our recent work [14,15] also demonstrated that using supersonic flow ionization by high-voltage, short-pulse duration, high repetition rate pulsed discharge instead of RF discharge greatly improves plasma stability and allows generating significantly higher flow conductivities. However, these experiments have left open the question whether the supersonic boundary layer under investigation was laminar or turbulent.

The main objectives of the present work are (i) to determine the state of the boundary layer at these conditions using laser sheet scattering flow visualization and laser differential interferometry (LDI) diagnostics and (ii) to detect the MHD effect using repetitively pulsed ionization, which may result in better flow control authority due to producing higher conductivities.

2. Experimental

The experiments have been conducted at the supersonic nonequilibrium plasma/MHD wind tunnel facility at the Nonequilibrium Thermodynamics Laboratories [9,13-15]. Briefly, this facility generates stable and diffuse supersonic nonequilibrium plasmas flows at M=3-4 in a uniform magnetic field up to B=2 T, with run durations from tens of seconds to complete steady state.

The schematic of the supersonic nozzle and a M=3 MHD test section is shown in Fig. 1. An aerodynamically contoured M=3 supersonic nozzle made of transparent acrylic plastic is connected to a 2 cm x 4 cm rectangular cross section test section 12 cm long with an angle step diffuser. The nozzle / test section / diffuser assembly is attached to a vacuum system connected to a 1200 ft^3 dump tank pumped out by an Allis-Chalmers 1300 cfm rotary vane vacuum pump. The minimum pressure in the vacuum system sustained by the pump is 35-40 torr, which necessitates the use of a supersonic diffuser with the nozzle / test section operated at relatively low stagnation and static pressures (P_0=1/3-1 atm, P_{test}=7-20 torr). The nozzle assembly is equipped with pressure taps measuring plenum pressure as well as static pressures at the beginning and at the end of the test section. The nozzle throat dimensions are 20 mm x 9.5 mm, which gives a mass flow rate through the test section of $\dot{m}$=15 g/sec at P_0=1/3 atm.

Two rectangular electrode blocks 5 cm long are flush mounted in the side test section walls (see Fig. 1). Each electrode block, made of mica ceramic, incorporates a single copper plate electrode 35 mm wide, 45 mm long, and 3 mm thick. The electrode edges are rounded using a Rogowski profile [16] to achieve a more uniform electric field distribution between the electrodes. To accommodate the electrodes, recesses are machined in the ceramic blocks. This creates a 2 mm thick ceramic layer between each electrode and the flow in the test section. On the opposite sides, the electrodes are covered with 2 mm thick acrylic plates. The gaps between the copper electrodes, the ceramic blocks, and the cover acrylic plates are filled with a self-hardening dielectric compound to preclude electrode surface exposure to air and prevent corona formation near the high-voltage electrode surface. Figure 2 shows a photograph of the M=3 test section.

Ionization in the test section is produced using a Chemical Physics Technologies custom designed high-voltage (up to 25-30 kV peak), short pulse duration (~10-20 nsec), high repetition rate (up to 50 kHz) pulsed plasma generator. The plasma generator produces high voltage pulses by compressing 500 V peak, 1 μsec long input pulses using several stages of magnetic compression circuits. The use of the insulated gate bipolar transistor switch allows reaching high pulse repetition rates. During the pulser operation, current and voltage in the pulsed discharge are measured using a Tektronix P6015A high voltage probe and a low-capacitance resistive current probe.

Transverse DC electrical current (sustainer current) in the supersonic flow ionized by the repetitively pulsed discharge is sustained by applying a DC field (up to 500 V/cm) to two 50 mm x 20 mm DC electrode blocks flush mounted in the top and bottom nozzle walls 4 cm apart, perpendicular both to the flow velocity and to the magnetic field direction, as shown in Fig. 1. The applied DC field, which is far too low to produce additional ionization in the flow, except in the cathode layer, is needed to sustain transverse (MHD) current. The DC electrode blocks are made of boron nitride ceramic, with continuous copper electrodes 45 mm long each. The transverse DC field is applied using a DEL 2 kV / 3A power supply operated in a voltage stabilized mode, with a 0.5-2.0 kΩ ballast. Two inductors 1 mH each were placed in the DC circuit in series with both DC electrodes to attenuate high amplitude current pulses propagation into the DC circuit. Current in the DC sustainer circuit is measured using a Tektronix AM503S current probe.

In the present work, some plasma characterization measurements have been done in a M=4 MHD test section with the same dimensions and same electrodes as in the M=3 test section. The M=4 contoured nozzle throat dimensions are 20 mm x 3.2 mm, which gives the mass flow rate of $\dot{m}$=15 g/sec at P_0=1 atm.

The entire nozzle / test section / diffuser assembly was placed between the poles of a GMW water cooled electromagnet, as shown in Figs. 1, 2, and attached to a 4 foot long, 6 inch diameter PVC vacuum pipe connected to the vacuum system. To improve the pulsed discharge load impedance matching, the high voltage pulse magnetic compression unit was also mounted inside

the magnet, above the test section (see Fig. 2), and short high voltage electrode cables (5 cm long) have been used. The magnet can generate a steady-state magnetic field up to B=3.5 T between two circular poles up to 25 cm in diameter. In the present experiments, for the distance between the 15 cm diameter poles of 6 cm, the magnetic field at maximum current through the magnet coils of 140 A is B=1.8 T. For relatively short run durations (of the order of tens of seconds), the magnetic field can be significantly increased by temporarily increasing the magnet current (up to ~200 A) and chilling the cooling water. To preclude external magnetic field penetration into the pulse compression unit, it was placed inside a custom-made six-layer shell magnetic shield made of a high magnetic permeability material with the total wall thickness of 1/2". Multiple layers are necessary because of the magnetic flux saturation in the outermost shield layers in the strong external magnetic field. At the B=1.5 T field between the magnet poles, the field inside the magnetic shield was about 20-30 mT. Mounting the pulse compression inside the magnetic shield also required the use of longer electrode cables (15 cm long), which adversely affected impedance matching.

Optical access to the flow in the test section is provided using two 1" x 1/2" glass windows in the top and bottom walls of the test section (see Fig. 1). The MHD effect on a supersonic ionized boundary layer was studied using a Laser Differential Interferometry (LDI) diagnostics described in greater detail in Ref. [17]. Briefly, a plane polarized He-Ne laser beam (Coherent He-Ne laser, model # 31-2025) is split into two circular polarized beams using a Wollaston prism (see Fig. 3) and sent through two different regions in the supersonic flow in the test section. The reference beam is passing through the flow along the centerline and the probe beam is passing through the boundary layer (see Fig. 3). The resultant phase shift between the two beams is proportional to the average density difference along the two beam paths. Therefore, Fourier transform of the resultant interference signal performed by a Stanford Research Systems (Model SR 785) Dynamic Signal Analyzer yields the boundary layer density fluctuation spectrum (relative to the reference laser beam passing through the centerline of the flow). The reference and the probe laser beam diameters, which limit the spatial resolution of the LDI signal, are approximately 2 mm each. The location of the probe beam can be controlled by rotating the prism. LDI signal acquisition, averaging, and processing by the signal analyzer requires a steady state flow run

time of several seconds, depending on the number of averages. Typically, good signal to noise is achieved for the acquisition / processing times of 1-2 sec.

As in our previous work [9,13-15], in the present MHD boundary layer control experiments, most LDI measurements are performed for both accelerating and decelerating Lorentz force directions. In both these cases, Lorentz force can be generated by two possible combinations of the transverse B field and the transverse DC electric field directions. Control runs in a cold supersonic flow without plasmas and in an ionized flow without DC electric field applied, i.e. when the time-averaged Lorentz force is zero, have also been conducted. The purpose of this approach was to isolate the MHD effect, which should depend on the Lorentz force direction, from the polarity-independent effect of Joule heat. To evaluate run-to-run variation of the LDI spectra, several runs (2 to 3) have been conducted for each set of conditions.

To visualize the boundary layer flow in the supersonic test section, a separate series of experiments has been conducted in air flows without plasmas, with the test section mounted outside the magnet. In these experiments, the air flow upstream of the nozzle plenum was seeded with acetone vapor, which condensed into small droplets in the cold M=3 supersonic core flow in the test section but remained in the vapor state in relatively warm boundary layer flows. A pulsed Nd:YAG laser operated at 10 Hz repetition rate was used to generate a 1.5 cm wide laser sheet with the aid of two cylindrical lenses, which was then brought into the test section through the two optical access windows, as shown in Fig. 4. The laser sheet distance from the test section wall could be varied by moving a flat mirror (see Fig. 4). The laser light scattered on acetone droplets formed in the flow was captured through the transparent acrylic test section wall, in the direction perpendicular to both the laser sheet and the flow, as shown in Fig. 4. A Princeton Instruments PI-Max ICCD camera synchronized with the laser pulses has been used for this purpose.

3. Results and discussion

Figure 5 shows laser sheet scattering images of the side wall boundary layer in M=3 air flows, with the laser sheet positioned 2 mm from the test section wall. The images shown are for stagnation pressures ranging from P_0=150 torr to 450 torr. At these conditions, the flow Reynolds number ranges from $Re_x=2.7\cdot10^5$ to $8.1\cdot10^5$ (x=20 cm is the combined length of the supersonic nozzle and the test section, starting from the throat). To minimize the amount of laser light scattered off the windows coming into the camera, the top and bottom of the test section (5 mm distance from the top and the bottom walls) are masked. Therefore, the images visualize the flow region between x=19 and x=21 cm from the nozzle throat and h=5 mm and h=35 mm from the bottom wall. From Fig. 5, it can be seen that there is a significant warm region near the center plane of the flow with little or no scattering signal, which therefore appears dark. Regions above and below the center plane are illuminated, which indicates the presence of significant amounts of acetone droplets there and therefore lower temperature. The presence of the warm region near the test section center plane is consistent with the boundary layer bulge detected by our previous Pitot probe measurements [9,14], also predicted by the 3-D compressible Navier-Stokes flow code [18,19]. One can also see that as the stagnation pressure and the flow Reynolds number increase, the scattering signal distribution, which essentially maps the temperature field across the laser sheet, becomes increasingly chaotic, with the spatial scale of temperature variation regions (spots) gradually decreasing (see Fig. 5). At high stagnation pressures, the center plane boundary layer bulge nearly disintegrates. Similar results are observed for a laser sheet positioned 4 mm from the wall (see Fig. 6).

Scattering images obtained with the laser sheet positioned further away from the wall (6 mm and 8 mm), shown in Figs. 7 and 8, respectively, demonstrate presence of a few warm spots near the center plane of the flow (at 6 mm), or none at all (at 8 mm). This is again in good agreement with our previous Pitot probe and schlieren measurements [9,13,14], which both indicate the boundary layer thickness of approximately 6 mm, with maximum thickness near the center plane. Summarizing, the flow visualization results shown in Figs. 5-8 are consistent with the Pitot probe and schlieren data and lead us to conclude that as the flow Reynolds number increases, the boundary layer flow becomes less regular and more chaotic, with the density fluctuation spatial scale decreasing. This suggests characterizing the boundary layer in the

stagnation pressure range of P_0=150 torr to 450 torr as transitional from laminar at the lower stagnation pressures to turbulent at the higher stagnation pressures.

Figure 9 compares a laser sheet scattering image of a boundary layer in a M=3 air flow at a stagnation pressure of P_0=150 torr with the flow temperature distribution calculated by solving laminar three-dimensional compressible Navier-Stokes equations [18]. Both images show vertical "slices" of the flow 2 mm away from the side wall of the test section. In both cases, the warmer region near the flow centerline (a boundary layer bulge) can be clearly seen. One can also see that the width of the bulge predicted by the code is consistent with the flow visualization results. Comparison of a laser sheet scattering image of M=3 boundary layer flow with the calculated temperature distribution [18], and with the contour plot of the Mach number [19] at a higher stagnation pressure, P_0=250 torr, is shown in Fig. 10. As in Fig. 9, first two images show vertical "slices" of the flow 2 mm away from the wall, while the third image shows the contour plot of the Mach number at x=20. Again, the warmer region (lower Mach number) near the flow centerline can be seen in all three cases. Note tat the predicted width of the boundary layer bulge at these conditions is smaller than at P_0=150 torr, which is again consistent with the results of the flow visualization (compare Figs. 9 and 10).

LDI spectra in M=3 air flows without plasmas have been measured in the same stagnation pressure range, P_0=150-500 torr. Figures 11 and 12 plot the spectra measured with the probe laser beam located 2 mm and 4 mm from the test section wall, i.e. at the conditions of Fig. 5 and Fig. 6, respectively. Note that due to the finite He-Ne laser beam diameters the LDI signal is actually collected from regions 2±1 mm and 4±1 mm from the wall, respectively. It can be seen that although the flow scattering images change quite significantly as the stagnation pressure is increased (see Figs. 5, 6), the overall shape of the LDI spectra, with an extended plateau and a steep roll-off at high frequencies, does not exhibit such dramatic changes (see Fig. 11, 12). Therefore, compared to laser scattering flow visualization, detection of turbulent transition based on the interpretation of LDI spectra alone is somewhat problematic. However, the behavior of the LDI signal intensity at 10 kHz (i.e. in the plateau region of the spectra), plotted vs. stagnation pressure in Figs. 13, 14 and showing a steep increase up to P_0≈200-250 torr with subsequent leveling off, appears more systematic. Based on both the laser scattering images shown in Figs.

5,6 and the LDI signal plotted in Figs. 13,14, we conclude that turbulent transition in the M=3 boundary layers on the side walls occurs at stagnation pressures of $P_0 \approx 200$-250 torr.

Fig. 15 shows photographs of crossed discharges (repetitively pulsed discharge + DC sustainer discharge) in M=4 flows of nitrogen (at B=0) and air (at B=1.5 T) at P_0=1 atm. In both cases, the pulse repetition rate is ν=40 kHz. Visual observation of the pulsed/DC discharges showed that in both cases the plasma is stable and uniform, without the "hot spots" appearing in the test section corners, which occurred in transverse RF discharge in supersonic flows [9,13]. Figures 16, 17 show single pulse voltage oscillograms in M=4 nitrogen flows at P_0=1 atm, P_{test}=10 torr, and in M=3 nitrogen flows at P_0=250 torr, P_{test}=7 torr, respectively, at different values of the magnetic field. From Fig. 16, it can be seen that using longer electrode cables (15 cm long instead of 5 cm long) noticeably reduced the output pulse amplitude, from nearly 20 kV to about 15 kV. In addition, applying a 1.5 T magnetic field resulted in distortion of the pulse due to partial field penetration through the magnetic shield, and in further amplitude reduction to about 11 kV. In M=3 flows, the pulse amplitude remained nearly the same, approximately 15 kV, for the fields up to B=1.25 T (see Fig. 17). At B=1.5 T, the peak voltage was reduced to about 12 kV, with pulse duration (FWHM) approximately 30 ns, again due to magnetic field penetration through the shield.

Figure 16 shows oscillograms of voltage and current between the DC sustainer (MHD) electrodes in a pulse-ionized M=3 nitrogen flow at P_0=250 torr, P_{test}=7.5 torr, B=1.5 T, DC power supply voltage of U_{PS}=2 kV, and ballast resistor of R=1 kΩ. Since the DC power supply operates in the voltage stabilized mode, the voltage between the DC electrodes is $U=U_{PS}-IR$, where I is the sustainer current. In this figure, the current pulse produced during the high voltage pulses is not resolved. It can be seen that the peak MHD current reaches about I=1.25 A after each pulse, with the subsequent fall-off in a decaying plasma between the pulses, to a minimum value of about I=0.5 A. Note that the plasma does not fully decay between the pulses. The time-averaged current and voltage at these conditions are $\langle U \rangle$=1.27 kV and $\langle I \rangle$=0.73 A. The time-averaged DC power coupled to the nitrogen flow at these conditions is quite substantial, about 1 kW, which in case of instant thermalization would result in the estimated flow temperature rise of about ΔT=60 K, from the baseline core flow temperature at M=2.9 of T=110 K. However, at

the reduced electric field in the sustainer discharge of $E/N=3\cdot10^{-16}$ V·cm^2 (based on the initial core flow temperature), more than 90% of the sustainer discharge input power goes to vibrational excitation of nitrogen [20], whose vibrational relaxation rate is extremely slow [21]. The slow vibrational relaxation rate locks up the energy stored in nitrogen vibrations and makes the supersonic flow essentially frozen. At similar discharge conditions in dry air, in spite of a high energy fraction input into vibrational excitation of nitrogen [20], vibrational relaxation of N_2 is much more rapid, primarily on O atoms produced in the plasma [21], which would result in a more significant Joule heating of the flow.

Figure 18 shows sustainer (MHD) currents in M=3 dry air flows at P_0=250 torr, P_{test}=7.5 torr, DC power supply voltage of U_{PS}=1.6 kV, and ballast resistor of R=1 kΩ. The current oscillograms are shown at different values of the magnetic field. It can be seen that the current decay rate in dry air is similar to that of nitrogen (compare Figs. 18 and 19). One can also see that the current decreases as the magnetic field is increased. This occurs due to the Hall effect, which in the case of continuous MHD electrodes generates the axial and reduces the transverse current component [22]. For the high values of the MHD loading parameter, $K=E_y/uB_z\sim40$, at the present conditions, the transverse and axial current components are given as follows,

$$I_y=\frac{\sigma}{1+\beta^2}E_yA \quad , \quad I_x=\beta\frac{\sigma}{1+\beta^2}E_yA \quad . \tag{3}$$

In Eqs. (3), σ is the scalar electric conductivity, A=10 cm^2 is the total surface area of the DC electrodes, and $\beta=eB_z/m_e\nu_{en}$ is the Hall parameter, i.e. the ratio of the electron cyclotron frequency, eB_z/m_e, to the electron-neutral collision frequency, ν_{en}. Transverse electric field in Eqs. (3) can be estimated as $E_y\cong(U-U_c)/h$, where $U=U_{PS}-IR$, U_c is the cathode voltage fall and h=4 cm is the test section height. From Eqs. (3), one can also obtain the following expression for the current voltage characteristic of the MHD sustainer discharge,

$$I=\sqrt{I_x^2+I_y^2}=\frac{\sigma}{\sqrt{1+\beta^2}}(U-U_c)\frac{A}{h} \quad . \tag{4}$$

Since the flow conductivity, generated by the repetitively pulsed discharge, is independent on the DC sustainer voltage, Eq. (4) shows that the conductivity and the Hall parameter can be determined by measuring current voltage characteristics of the non-self-sustained DC discharge at different values of the magnetic field.

Figures 20 and 21 show current voltage characteristics of the MHD sustainer discharge in M=3 flows of nitrogen and dry air at P_0=250 torr and P_{test}=7.5 torr. It can be seen that at low voltages the sustainer current remains very low and nearly independent of the applied voltage, while at high voltages the current exhibits linear voltage dependence, as expected for the constant conductivity plasma. Basically, if the applied voltage is low, the voltage across the cathode layer of the discharge is insufficient to accelerate ions toward the cathode, release enough secondary electrons from the cathode surface, and sustain a significant current, even at the conditions when the conductivity in the positive column of the discharge is high. The cathode voltage falls for different B fields were determined from the x-axis intercept of the linear slope of the current voltage characteristics, as shown in Figs. 20,21. At the absence of magnetic field, the cathode falls in nitrogen and in air are U_c=260±50 V and U_c=350±50 V, which is close to the normal glow discharge cathode fall, 208 V in nitrogen and 370 V in air (both for copper cathode) [20]. The present measurements show that both in nitrogen and air, the cathode fall increases with the magnetic field, up to U_c=500±50 V and U_c=520±50 V at B=1.5 T in nitrogen and air, respectively (see Figs. 20,21). Qualitatively, this can be explained by the reduction of the ion current to the cathode and therefore reducing the secondary electron emission from the cathode due to the Hall effect, when the applied magnetic field is perpendicular to the current direction.

The electrical conductivity of the flow was found from the linear slope of the current voltage characteristics at B=0 (i.e. at β=0) using Eq. (4), σ=0.073 mho/m in nitrogen and σ=0.072 mho/m in air. Finally, assuming that the conductivity is independent of the magnetic field, the Hall parameter was determined from the current-voltage characteristics slopes at B=0.75 T and B=1.5 T in nitrogen, (β=1.15 and 1.6, respectively), and at B=1.5 T in air (β=2.1), also using Eq. (4). The present conductivity and Hall parameter measurements are more accurate than our previous results [9,14,23], since in our previous work systematic measurements of the current

voltage characteristics and of the cathode voltage fall have not been conducted. In addition, in our previous experiments [9,23] the transverse RF discharge geometry was rather complicated, which made discharge characterization difficult.

Figure 22 shows the LDI spectra in M=3 flows of nitrogen at the plenum pressure of P_0=250 torr, magnetic field B=1.5 T, sustainer voltage U_{PS}=2 kV, and the LDI probe beam placed 6 mm from the wall, i.e. near the outer edge of the boundary layer (see Figs. 5-8). The two groups of spectra shown are for the ballast resistor of R=1 kΩ (time averaged MHD current of <I>=0.65 A) and R=0.5 kΩ (<I>=0.94 A), both for accelerating and retarding Lorentz force directions. It can be seen that at the lower MHD current, there is almost no effect of the Lorentz force polarity on the density fluctuations, while at the higher MHD current, the retarding force results in higher density fluctuation intensity in the frequency range of 2-40 kHz, up to 2 dB (about 25%). For both accelerating and retarding force, the results of two successive runs are shown to demonstrate the run-to-run reproducibility of the observed effect, which appears to increase with the MHD current.

Figure 23 shows the LDI spectra in M=3 dry air flows at the same conditions as the high-current regime of Fig. 22, i.e. at R=0.5 kΩ, <I>=0.78 A. In this case, the four spectra shown correspond to four possible combinations of the MHD current and the magnetic field vectors, **j** and **B**, two of which correspond to the accelerating Lorentz force and the other two to the retarding Lorentz force, **F=jxB**. This has been done by switching the DC power supply polarity and/or the magnet power supply polarity. One can see that both retarding force combinations produce significantly higher density fluctuation intensities in the frequency range of 2-40 kHz compared to both accelerating force combinations, again up to 2 dB.

Figures 22 and 23 also show LDI spectra measured with the pulsed power supply operating but with the DC sustainer voltage turned off, i.e. when there was no MHD force applied to the flow. It can be seen that at these conditions the density fluctuation spectra are very close to the spectra measured with the accelerating MHD force applied. It was also found that the LDI spectra measured in both nitrogen and air flows without plasmas (i.e. with both power supplies turned off) are nearly identical to the spectra with only the pulser operating. These results show that in

both cases the effect on the density fluctuations is detected only when the retarding MHD force is applied to the flow, as well as provide strong evidence that the observed effect is indeed due to Lorentz force, not Joule heating of the flow.

Qualitatively, the observed density fluctuation increase by the retarding Lorentz force appears to be consistent with the results of turbulence measurements in a M=3 turbulent boundary layer in the presence of an adverse pressure gradient [24], which showed that at these conditions the turbulence intensity, $\overline{u'^2}$, $\overline{v'^2}$, and turbulent shear stress, $\overline{u'v'}$, are all significantly amplified. However, the authors of Ref. [24] suggest that these results should be interpreted with caution. Indeed, turbulence measurements in a M=3 turbulent boundary layer in a rapid expansion flow (i.e. in the presence of an accelerating pressure gradient) [25] showed that although the turbulence intensity, $\overline{u'^2}$, at these conditions is significantly reduced, the mass flux fluctuations, $\overline{\rho' u'}$, remain unchanged, which suggests that density fluctuations, $\overline{\rho'}$, are also unlikely to change. Interestingly enough, in the present work we also have not found any detectable effect of accelerating Lorentz force on the density fluctuations.

In the present measurements, the highest time-averaged MHD sustainer currents, exceeding 1 A, were detected in M=3 flows of N_2-He mixtures. Figure 24 shows the density fluctuations spectra in M=3 flows of a 80% N_2 – 20% He mixture, at P_0=250 torr, magnetic field B=1.5 T, sustainer voltage U_{PS}=2 kV, and R=0.5 kΩ. At these conditions, the time averaged MHD current was <I>=1.02 A for the accelerating Lorentz force and <I>=1.14-1.17 A for the retarding force. The LDI spectra shown in Fig. 24 have been measured at two different distances from the test section wall, 6 mm and 4 mm. Again, in both these cases, the results are consistent with measurements in nitrogen and air, i.e. the density fluctuation intensity is noticeably higher (by up to 2 dB) for the retarding Lorentz force. This final series of measurements demonstrate that the MHD effect on the density fluctuations is detected at multiple locations across the boundary layer.

4. Summary and future work

This work presents results of supersonic boundary layer flow visualization experiments using laser sheet scattering, as well as MHD boundary layer control experiments using repetitively pulsed, short pulse duration, high voltage discharge in M=3 flows of nitrogen and air in the presence of magnetic field of B=1.5 T. Laser sheet scattering experiments using flow seeding with acetone vapor showed that side wall boundary layers in the supersonic test section are considerably thicker near the center plane of the flow. Boundary layer thickness determined from the flow visualization is consistent with previous Pitot probe and schlieren measurements. The flow visualization results also show that as the stagnation pressure increases from P_0=150 torr to 450 torr, for Reynolds number ranging from $Re_x=2.7\cdot10^5$ to $8.1\cdot10^5$, the boundary layer flow becomes much more chaotic, with the spatial scale of temperature fluctuations decreasing. Combined with the results of density fluctuation spectra measurements using the Laser Differential Interferometry (LDI) diagnostics, this behavior suggests that boundary layer turbulent transition occurs at stagnation pressures of P_0~200-250 torr.

Operation of a crossed discharge (pulser + DC sustainer) in M=3 flows of air and nitrogen at the pulse repetition rate of 40 kHz demonstrated that such discharge produces a stable, diffuse, and uniform plasma. The peak voltage in the repetitively pulsed discharge used for supersonic flow ionization in the present experiments is about 12 kV, with the voltage pulse duration (FWHM) of approximately 30 ns. Both in nitrogen and in dry air, the plasma does not fully decay between the ionizing high voltage pulses. The time-average DC current achieved in such discharges is up to 1.0 A in nitrogen (conductivity of σ=0.073 mho/m) and up to 0.8 A in air (σ=0.072 mho/m). The electrical conductivity and the Hall parameter in nitrogen and air flows are inferred from the current voltage characteristics of the sustainer discharge. These results demonstrate feasibility of the use of the repetitively pulsed discharge as an efficient and stable ionization source sustaining electrical conductivity in supersonic nonequilibrium MHD flows.

LDI measurements detected an MHD effect on the ionized boundary layer density fluctuations at these conditions. In particular, retarding Lorentz force applied to M=3 nitrogen, air, and N_2-He flows produces an increase of the density fluctuation intensity by up to 2 dB (about 25%), compared to the accelerating force of the same magnitude applied to the same flow. The effect is demonstrated for two possible combinations of the magnetic field and transverse current

directions producing the same Lorentz force direction (both for accelerating and retarding force). Comparison with the LDI spectra measured with no MHD force applied showed that the effect on the density fluctuations is produced only by the retarding Lorentz force, while the Joule heat effect appears insignificant.

In future work, the main thrust will be to improve the flow quality in the MHD test section. This will include design and manufacturing of two new M=3 and M=4 test sections with the contoured nozzle walls, as well as angle step diffuser walls being the side walls of the test section (instead of top and bottom walls in the present design). In this new design, small divergence angle will also be introduced between the side walls to provide boundary layer relief. These changes are expected to considerably reduce the secondary cross flow producing bulges in the side wall boundary layers. Finally, since seeding the flow with acetone vapor is not feasible in the presence of plasmas in the test section, a long-term objective is also to develop *in situ* boundary layer flow visualization diagnostics, which can be used to characterize the state of the boundary layer during the MHD forcing. A promising possibility in this respect is seeding the flow with nitric oxide and using laser sheet NO LIF on the 226 nm NO($X^2\Pi$, v=0 $\rightarrow$ $A^2\Sigma$, v=0) γ-band transition to map the flow temperature field.

6. References

1. Adamovich, I.V., Rich, J.W., and Nelson, G.L. "Feasibility Study of Magneto-hydrodynamics Acceleration of Unseeded and Seeded Air Flows", AIAA Journal, Vol. 36, No. 4, 1998, pp. 590-597
2. Fraishtadt, V.L., Kuranov, A.L., and Sheikin, E.G. "Use of MHD Systems in Hypersonic Aircraft," Technical Physics, Vol. 43, No. 11, 1998, pp. 1309-1314
3. Park, C., Mehta, U.B., and Bogdanoff, D. W., "Magnetohydrodynamic Energy Bypass Scramjet Performance with Real Gas Effects", Journal of Propulsion and Power, Vol. 17, No. 5, 2001, pp. 1049-1057
4. Macheret, S.O., Shneider, M.N., Miles, R.B., and Lipinski, R.J., "Electron Beam Generated Plasmas in Hypersonic MHD Channels", AIAA Journal, Vol. 39, No.6, 2001,

pp. 1127-1136

5. Macheret, S.O., Shneider, M.N., and Miles, R.B., "Magnetohydrodynamic Control of Hypesonic Flow and Scramjet Inlets Using Electron Beam Ionization", AIAA Journal, Vol. 40, No.1, 2002, pp. 74-81
6. Macheret, S.O., Shneider, M.N., and Miles, R.B., "MHD Power Extraction from Cold Hypersonic Air Flow with External Ionizers", Journal of Propulsion and Power, Vol. 18, No. 2, 2002, pp. 424-431
7. Kuranov, A.L., and Sheikin, E.G., "Magnetohydrodynamic Control on Hypersonic Aircraft Under "Ajax" Concept", Journal of Spacecraft and Rockets", Vol. 40, No. 2, 2003, pp. 174-182
8. S.V. Bobashev, Yu.P. Golovachov, and D.M. Van Wie, "Deceleration of Supersonic Plasma Flow by an Applied Magnetic Field", Journal of Propulsion and Power, 2003, vol.19, no. 4, pp. 538-546
9. R. Meyer, M. Nishihara, A. Hicks, N. Chintala, M. Cundy, W.R. Lempert, I.V. Adamovich, and S. Gogineni, "Measurements of Flow Conductivity and Density Fluctuations in Supersonic Nonequilibrium MHD Flows", to be published in AIAA Journal, 2005
10. Palm, P., Meyer, R., Ploenjes, E., Bezant, A., Adamovich, I.V., Rich, J.W., and Gogineni, S., "MHD Effect on a Supersonic Weakly Ionized Flow", AIAA Paper 2002-2246, 33rd Plasmadynamics and Lasers Conference, Maui, HW, 20-23 May 2002
11. Schlichting, H., "Boundary Layer Theory", McGraw-Hill, New York, 1968, Chap. XXI
12. Henoch, C. and Stace, J., "Experimental Investigation of a Salt Water Turbulent Boundary Layer Modified by an Applied Streamwise Magnetohydrodynamic Body Force," Phys. Fluids, Vol. 7, No. 6, 1995, pp. 1371-1383
13. R. Meyer, N. Chintala, B. Bystricky, A. Hicks, M. Cundy, W.R. Lempert, and I.V. Adamovich, "Lorentz Force Effect on a Supersonic Ionized Boundary Layer", AIAA Paper 2004-0510, 42nd Aerospace Sciences Meeting and Exhibit, January 2004, Reno, NV
14. M. Nishihara, R. Meyer, M. Cundy, W.R. Lempert, and I.V. Adamovich, "Development and Operation of a Supersonic Nonequilibrium MHD Channel", AIAA Paper 2004-2441, 35th Plasmadynamics and Lasers Conference, Portland, OR, 29 June – 1 July 2004

15. M. Nishihara, N. Jiang, W.R. Lempert, I.V. Adamovich, and S. Gogineni, "MHD Supersonic Boundary Layer Control Using Pulsed Discharge Ionization", AIAA Paper 2005-1341, 43rd Aerospace Sciences Meeting and Exhibit, January 2005, Reno, NV
16. J. D. Cobine, "Gaseous Conductors: Theory and Engineering Applications", Dover Publications, New York, 1958
17. Salyer, T. R., Collicott, S. H., and Schneider, S. P., "Feedback Stabilized Laser Differential Interferometry for Supersonic Blunt Body Receptivity Experiments," AIAA-2000-0846, 38th AIAA Aerospace Sciences Meeting and Exhibit, Reno, NV, Jan. 2000
18. R. McMullan and M. Lindsey, I. Adamovich, and M. Nishihara, "Experimental Validation of 3-D Magnetogasdynamic Compressible Navier-Stokes Solver", AIAA-2004-2269, 35th AIAA Plasmadynamics and Lasers Conference, Portland, OR, June 28-1, 2004
19. P. Rawat, X. Zhong, V. Singh, and S. Gogineni, "Numerical Simulation of Secondary Flow in a Weakly Ionized Supersonic Flow with Applied Electromagnetic Field", AIAA Paper 2005-5050, 36th AIAA Plasmadynamics and Lasers Conference, Toronto, Ontario, June 6-9, 2005
20. Yu.P. Raizer, Gas Discharge Physics, Springer-Verlag, Berlin, 1991
21. B.F. Gordiets, V.A. Osipov, and L.A. Shelepin, "Kinetic Processes in Gases and Molecular Lasers", Gordon and Breach, London, 1988
22. Rosa, R.J., "Magnetohydrodynamic Energy Conversion", New York, McGraw-Hill, 1968
23. B. McEldowney, R. Meyer, N. Chintala, and I.V. Adamovich, "Measurements of Electrical Parameters of a Supersonic Nonequilibrium MHD Channel", AIAA Paper 2003-4279, 34th Plasmadynamics and Lasers Conference, Orlando, FL, 23-26 June 2003
24. E.M. Fernando and A.J. Smits, "A Supersonic Turbulent Boundary Layer in an Adverse Pressure Gradient", Journal of Fluid Mechanics, vol. 211, 1990, pp. 285-307
25. D.R. Smith and A.J. Smits, "The Rapid Expansion of a Turbulent Boundary Layer in a Supersonic Flow", Theoretical and Computational Fluid Dynamics, vol. 2, 1991, pp. 319-328

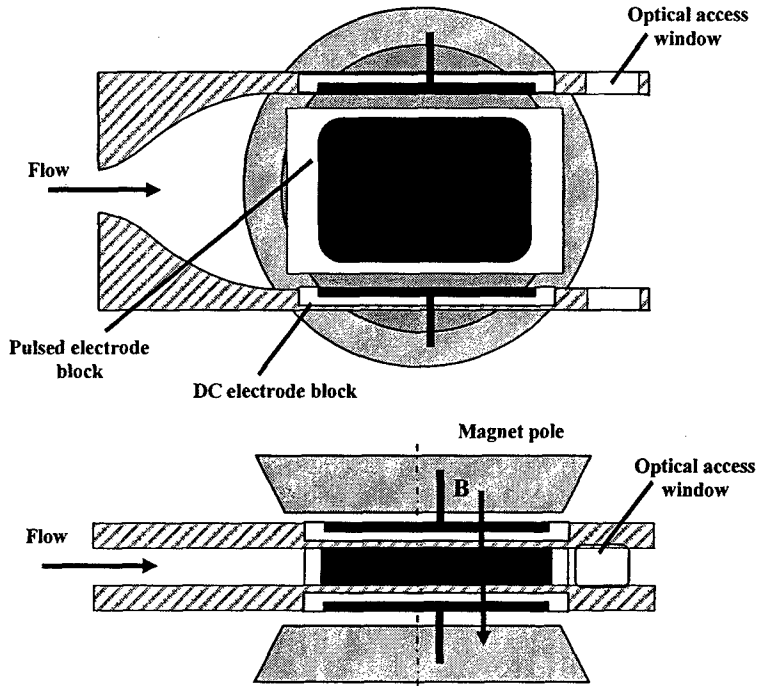

Figure 1. Schematic of a supersonic nozzle and MHD test section

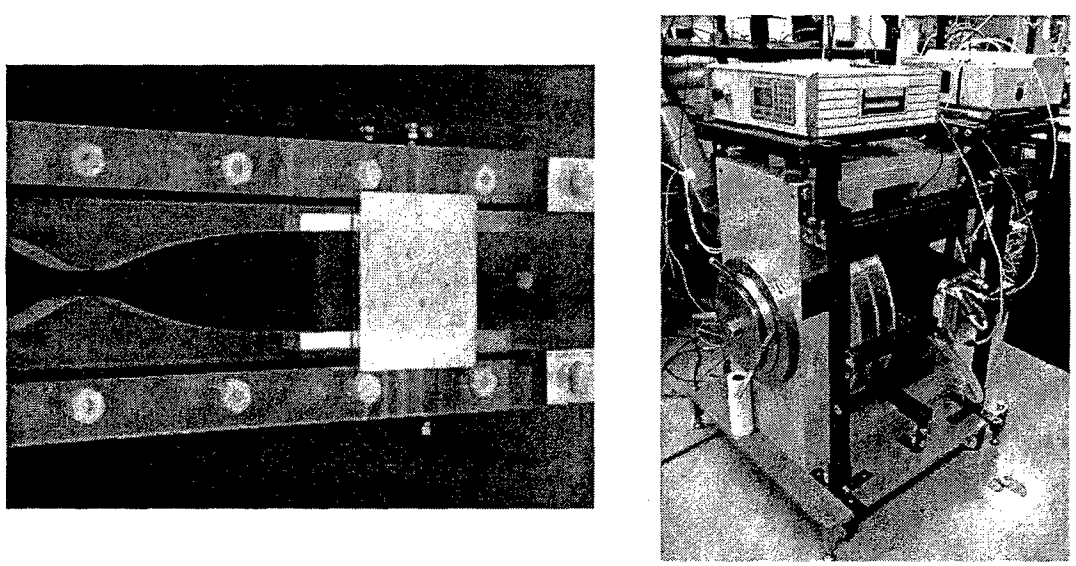

Figure 2. Photographs of a M=3 test section and of a high voltage pulse compression unit, mounted above the test section between the magnet poles.

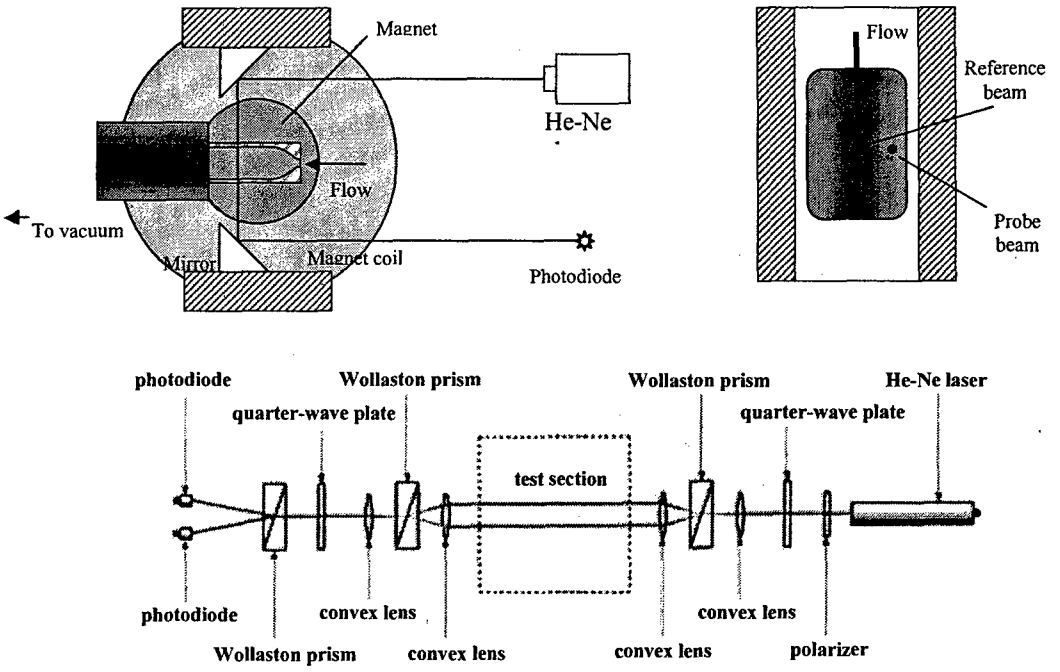

Figure 3. Layout and schematic of the LDI diagnostics

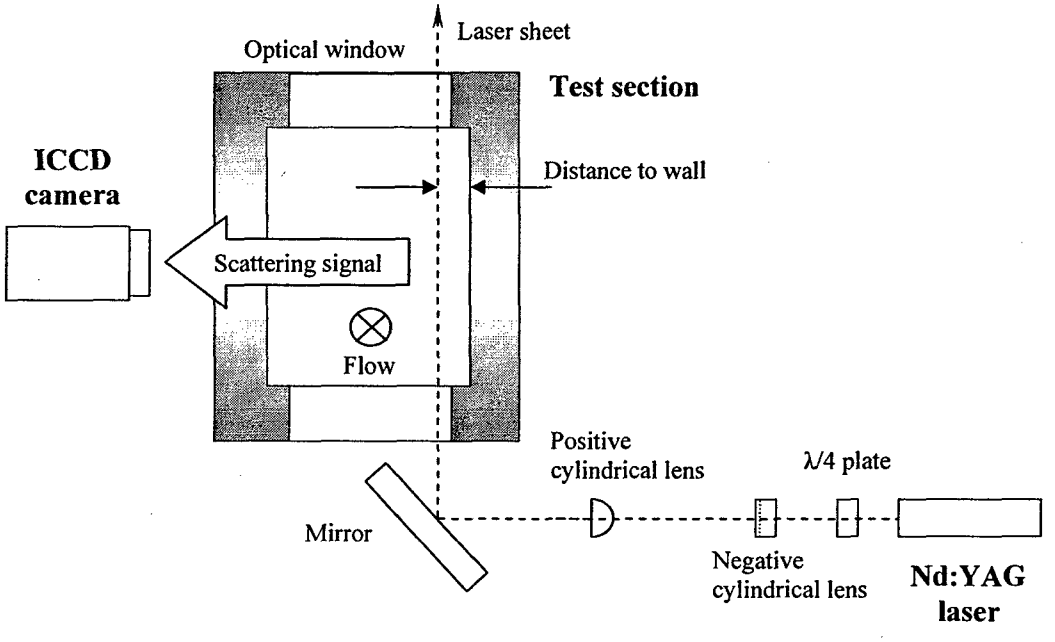

Figure 4. Schematic of the flow visualization experiment by laser sheet scattering

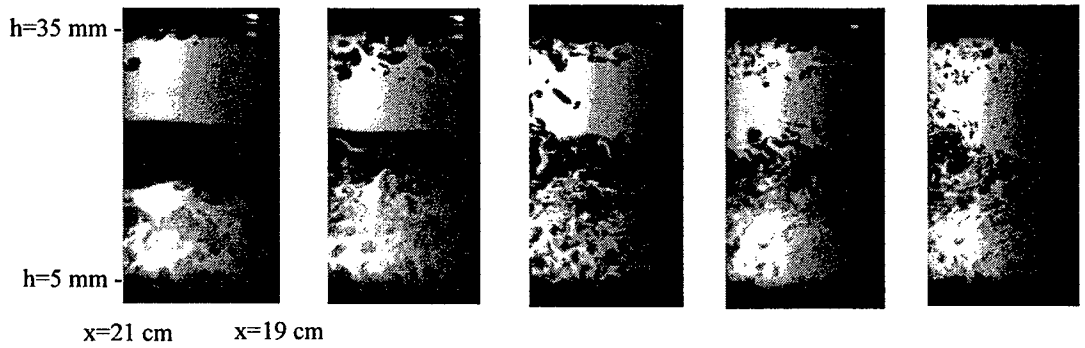

Figure 5. Laser sheet scattering images of a boundary layer in M=3 air flows, 2 mm away from the test section wall. Left to right, P_0=150 torr, 200 torr, 250 torr, 350 torr, and 450 torr (Reynolds number ranging from $Re_x=2.7\cdot10^5$ to $8.1\cdot10^5$).

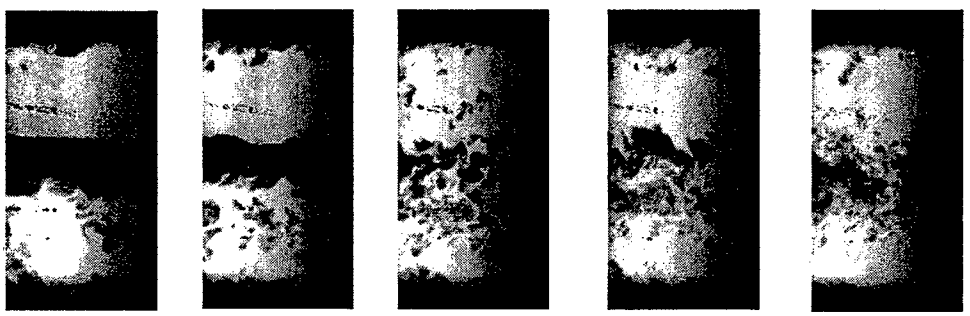

Figure 6. Laser sheet scattering images of a boundary layer in M=3 air flows, 4 mm away from the test section wall. Left to right, P_0=170 torr, 200 torr, 250 torr, 350 torr, and 450 torr. (Reynolds number ranging from $Re_x=3.1\cdot10^5$ to $8.1\cdot10^5$).

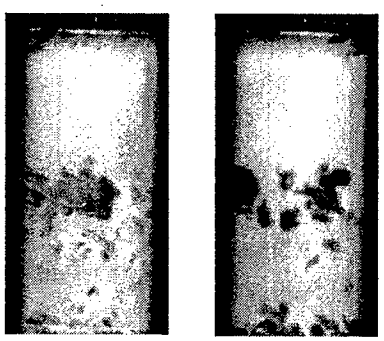

Figure 7. Laser sheet scattering images of a boundary layer in M=3 air flows, 6 mm away from the test section wall. Left to right, P_0=250 torr and 500 torr.

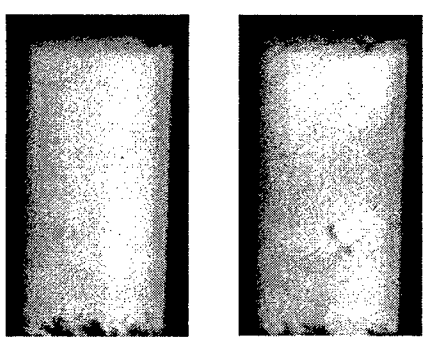

Figure 8. Laser sheet scattering images of a boundary layer in M=3 air flows, 8 mm away from the test section wall. Left to right, P_0=250 torr and 500 torr.

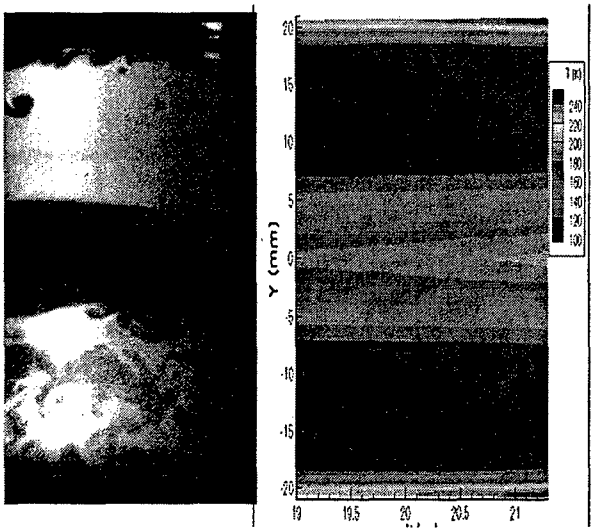

Figure 9. Comparison of a laser sheet scattering image of a boundary layer in a M=3 air flow (left) with the calculated temperature distribution [18] (right) 2 mm away from the wall, at P_0=150 torr. The warmer region near the centerline can be seen in both cases.

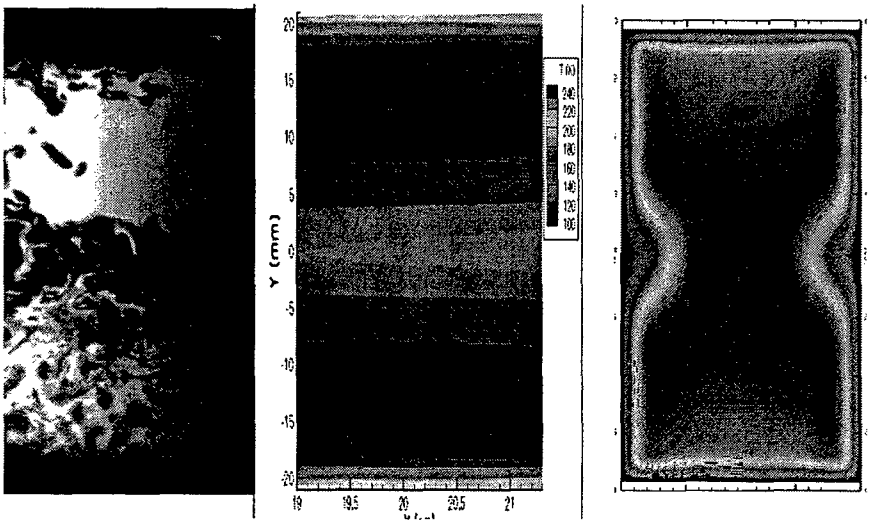

Figure 10. Comparison of a laser sheet scattering image of a boundary layer in a M=3 air flow (left) with the calculated temperature distribution [18] (center), and with the contour plot of the Mach number [19] (right). 2 mm away from the wall, P_0=250 torr. The warmer region (lower Mach number) near the centerline can be seen in all three cases.

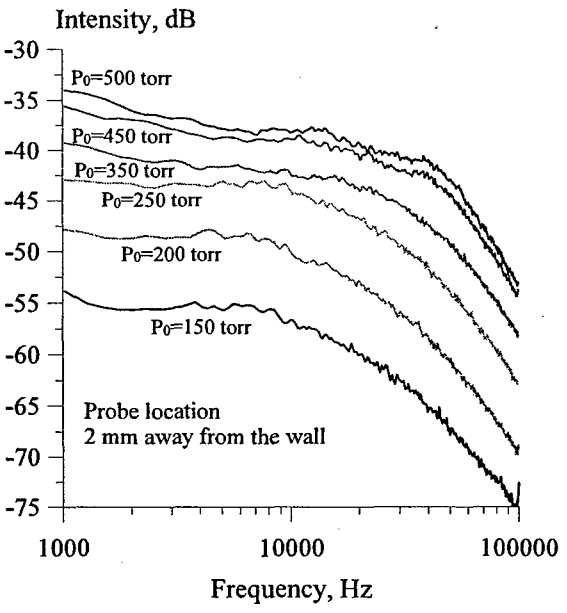

Figure 11. LDI spectra of M=3 air flows at different plenum pressures. The LDI probe beam is 2 mm away from the wall.

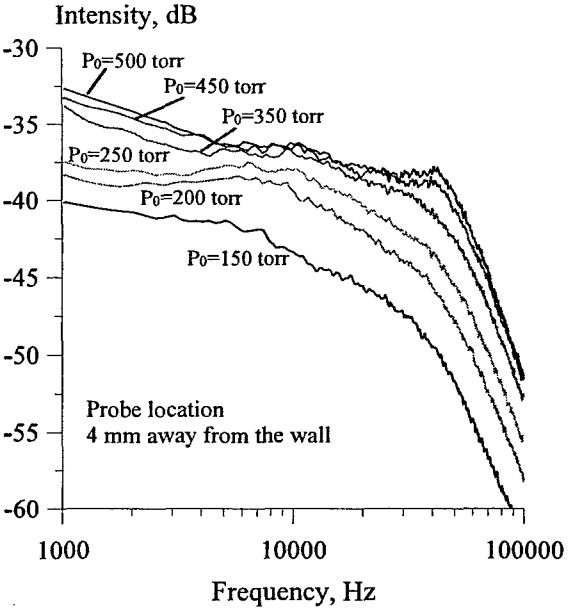

Figure 12. LDI spectra of M=3 air flows at different plenum pressures. The LDI probe beam is 4 mm away from the wall.

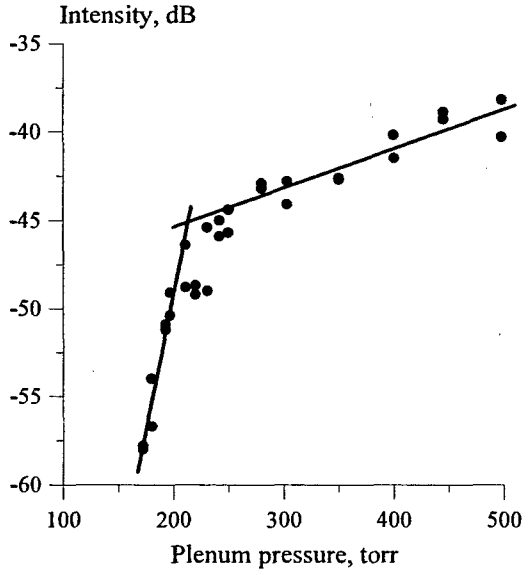

Figure 13. LDI signal intensity at a 10 kHz frequency as a function of plenum pressure for the conditions of Fig. 9 (the probe beam is 2 mm away from the wall).

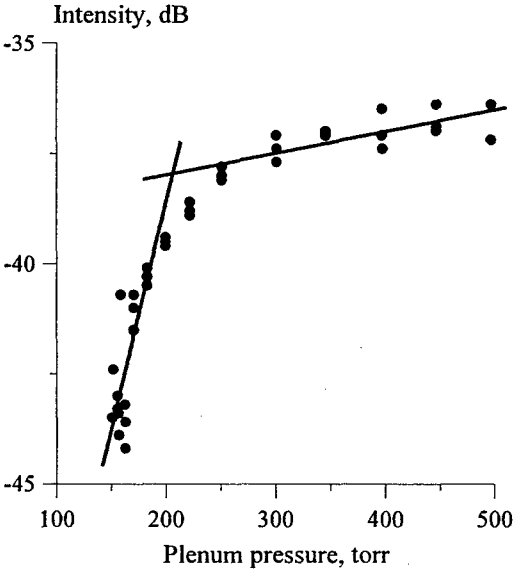

Figure 14. LDI signal intensity at a 10 kHz frequency as a function of plenum pressure for the conditions of Fig. 10 (the probe beam is 4 mm away from the wall).

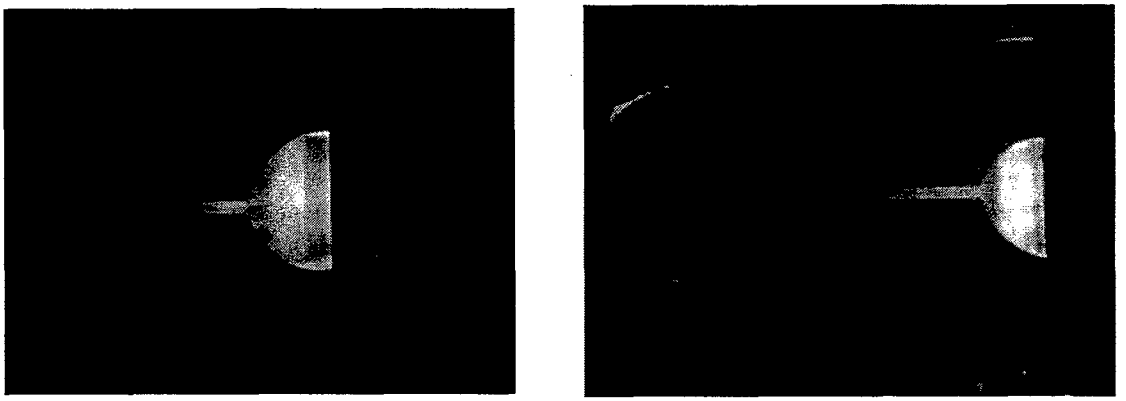

Figure 15. Photographs of pulsed discharges in M=4 flows at P_0=760 torr, P_{test}=10 torr, pulse repetition rate 40 kHz. **Left:** nitrogen, B=0; **right:** air, B=1.5 T. The discharge is seen at an oblique angle, looking in the direction of the flow.

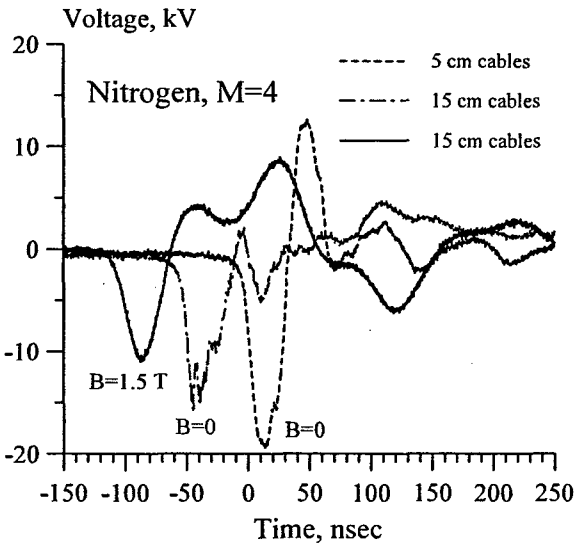

Figure 16. Single-pulse voltage oscillograms in M=4 nitrogen flows at P_0=1 atm, P_{test}=10 torr, for different values of magnetic field.

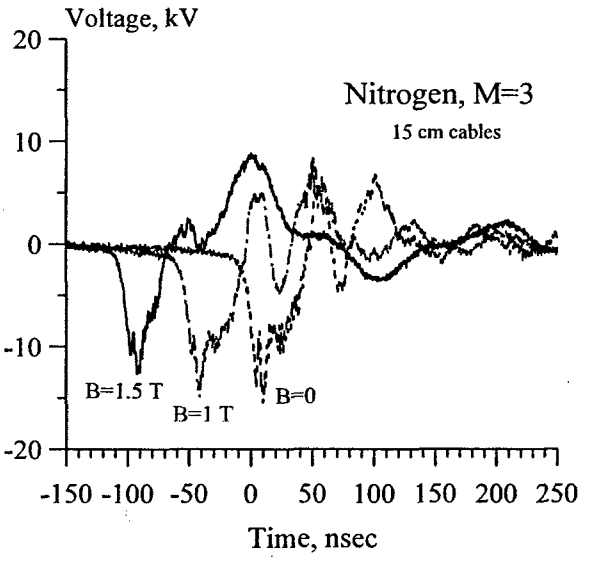

Figure 17. Single-pulse voltage oscillograms in M=3 nitrogen flows at P_0=250 torr, P_{test}=7 torr, for different values of magnetic field.

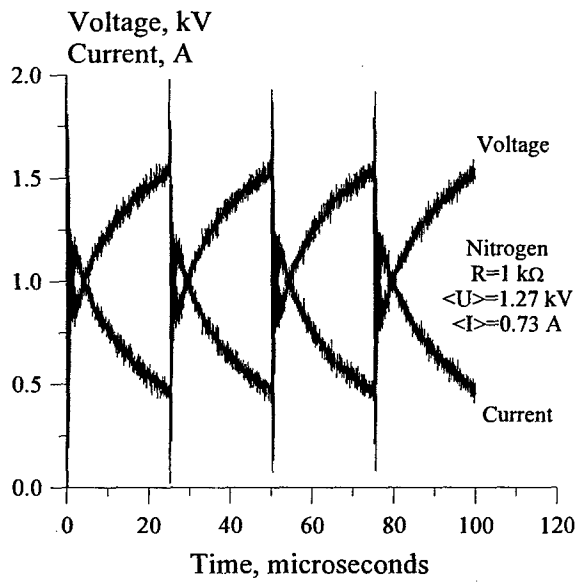

Figure 18. DC sustainer voltage and current oscillograms in a crossed discharge (pulser + DC) in a M=3 flow of nitrogen. P_0=250 torr, P_{test}=7.5 torr, pulse repetition rate 40 kHz. U_{DC}=2 kV, R= 1 kΩ, B=1.5 T.

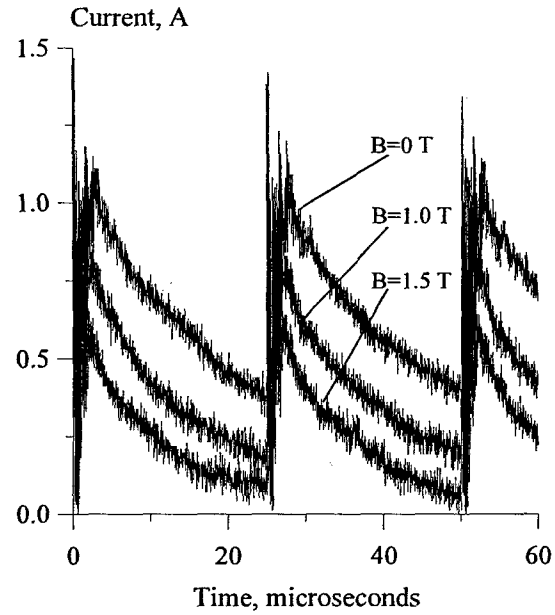

Figure 19. Current oscillograms in a crossed discharge (pulser + DC) in a M=3 flow of dry air for different values of magnetic field. P_0=250 torr, P_{test}=7.5 torr, pulse repetition rate 40 kHz. U_{DC}=1.6 kV, R= 1 kΩ.

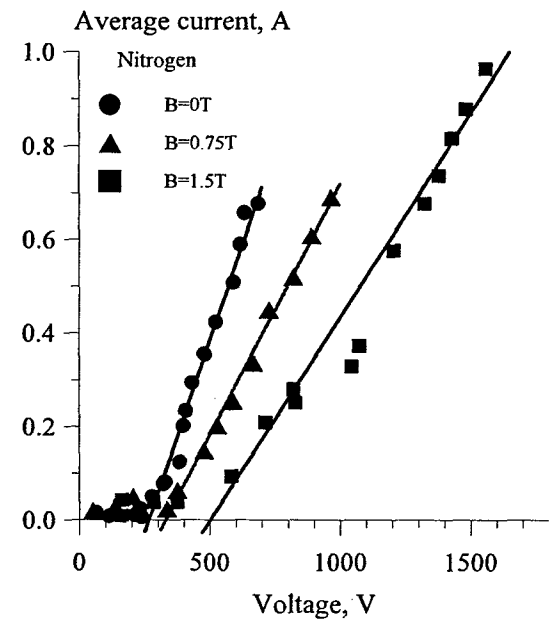

Figure 20. Current voltage characteristics of the sustainer discharge in M=3 flows of nitrogen at different values of magnetic field. P_0=250 torr, P_{test}=7.5 torr, pulse repetition rate 40 kHz.

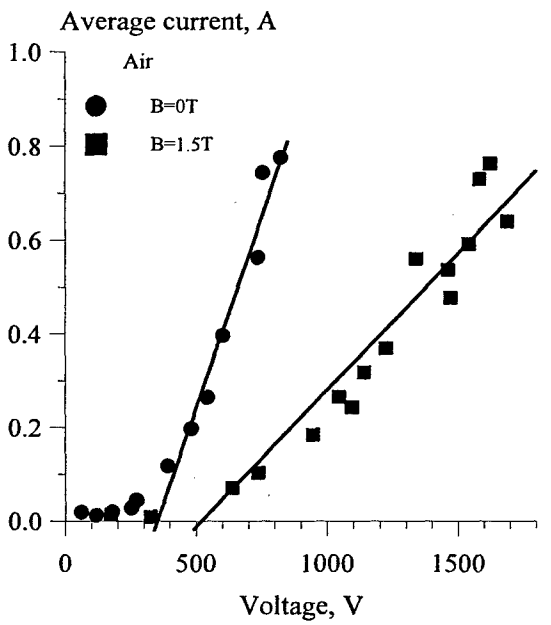

Figure 21. Current voltage characteristics of the sustainer discharge in M=3 flows of dry air at different values of magnetic field. P_0=250 torr, P_{test}=7.5 torr, pulse repetition rate 40 kHz.

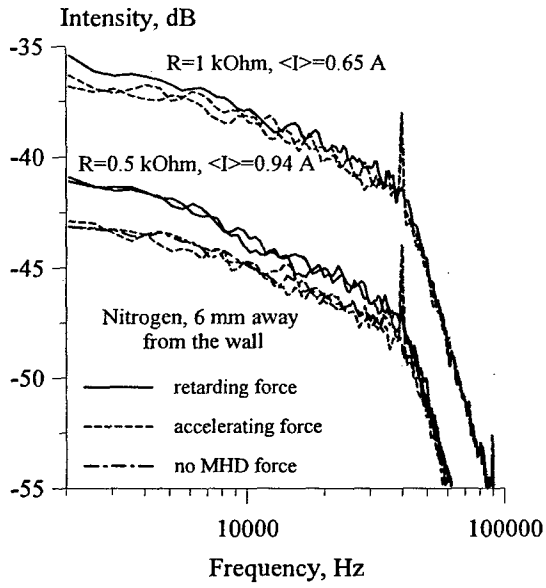

Figure 22. LDI spectra in a crossed discharge in a M=3 flow of nitrogen, for different Lorentz force directions and ballast resistances (MHD currents).

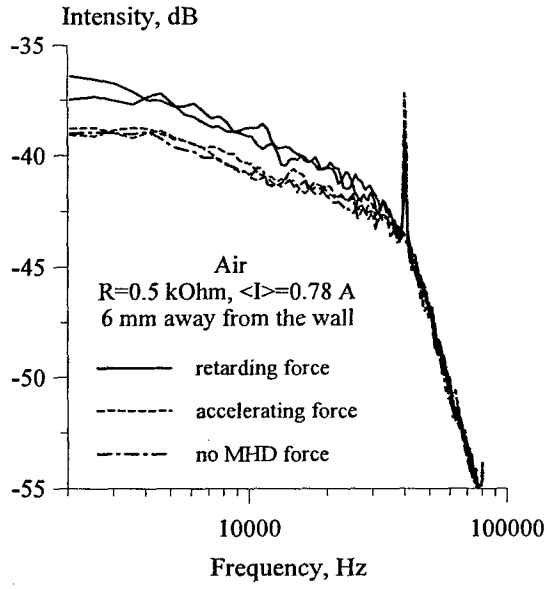

Figure 23. LDI spectra in a crossed discharge in a M=3 flow of dry air, for different Lorentz force directions. Both accelerating and retarding **jxB** force directions are created by two different combinations of **j** and **B** vectors.

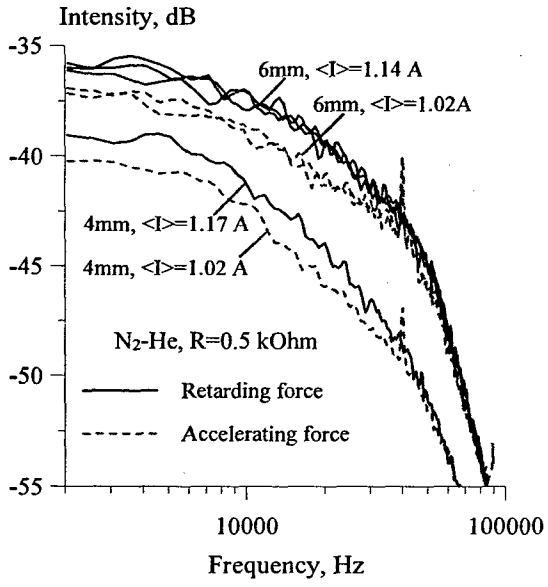

Figure 24. LDI spectra in a crossed discharge in a M=3 flow of an 80% nitrogen – 20% helium mixture, for different Lorentz force directions and LDI probe beam locations.